DEPARTMENT OF THE AIR FORCE

AIR UNIVERSITY

AIR FORCE INSTITUTE OF TECHNOLOGY

Wright-Patterson Air Force Base, Ohio

AFIT/GAE/ENY/91J-1

Experimental Evaluation of Design Variables for Two-Dimensional Confined Jet Thrust Vector Control Nozzles

THESIS

Timothy M. Hawkes

AFIT/GAE/ENY/91J-1

Approved for public release; distribution unlimited

AFIT/GAE/ENY/91J-1

Experimental Evaluation of Design Variables for Two-Dimensional Confined Jet Thrust Vector Control Nozzles

THESIS

Presented to the Faculty of the School of Engineering

of the Air Force Institute of Technology

Air University

In Partial Fulfillment of the

Requirements for the Degree of

Master of Science in Aeronautical Engineering

Timothy M. Hawkes, B.S.

June 1991

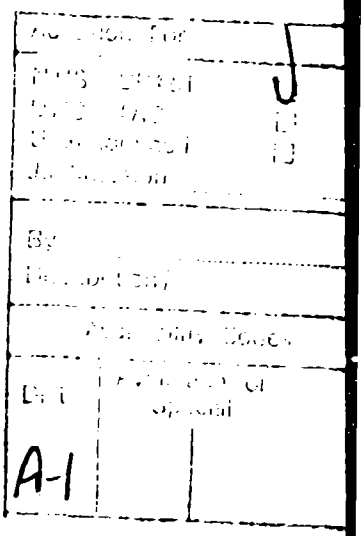

Approved for public release; distribution unlimited

Preface

The purpose of this study was to expand the database for two-dimensional (2-D) confined jet thrust vector control (CJTVC) nozzles. Variation in several design parameters were analyzed to determine their effect on the axial performance and vectoring ability of 2-D CJTVC nozzles. In addition, design guidelines for 2-D CJTVC nozzles were also established.

I would like to thank Dr. M. E. Franke for his support and patience throughout the entire study and also Dr. W. C. Elrod and Capt. P. S. Beran for their insightful comments during the preparation of this thesis. In addition, the technical support from the AFIT technicians and personnel of the model fabrication shop were invaluable to this study.

- Timothy M. Hawkes

Table of Contents

	Page
Preface	ii
List of Figures	v
List of Tables	viii
List of Symbols	ix
Abstract	xi
I. Introduction	1
Background	1
Objective	7
Approach	7
II. Experimental Apparatus	8
Nozzle Design	8
Nozzle Assembly	8
Test Stand	12
Primary and Secondary Flow Systems	12
Force Measurements	15
Static Pressure Measurements	17
Mass Flow Measurements	17
Temperature Measurements	17
Flow Visualization	18
Data Acquisition System	18
III. Experimental Procedure	19
IV. Results and Discussions	21
Baseline Results	21
Vectoring Performance	34
Effect of Exit Height	47
Effect of Port Location	47
Design Guidelines for CJTVC Nozzles	54
Effects of Ports on Axial Performance	57
V. Conclusions	63
VI. Recommendations	65
Appendix A: Uncertainty Analysis	66

Appendix B: Ideal Thrust Calculations..... 69

Appendix C: Calculation of Flow Separation Point..... 71

Appendix D: Measurements of the Flow Separation Point . 73

Bibliography..... 85

Vita 87

List of Figures

Figure		Page
1.	Illustration of BLTVC Operating Modes.....	3
2.	Illustration of CJTVC Operating Modes.....	4
3.	CJTVC Design Variables.....	9
4.	Photograph of Nozzle Test Assembly.....	11
5.	Photograph of Test Stand.....	13
6.	Schematic of Test Stand.....	14
7.	Photograph of Force Balance.....	16
8.	Nozzle Stability During Axial Tests, No Secondary Ports.....	22
9.	Nozzle Axial Efficiency, No Secondary Ports, Length=5".....	23
10.	Nozzle Axial Efficiency, No Secondary Ports, Length=4".....	24
11.	Effect of Expansion Ratio (Ae/At) on Nozzle Axial Efficiency, No Secondary Ports.....	26
12.	Static Pressure Distribution, Nozzle 53528, No Secondary Ports.....	28
13.	Flow Separation Point, Comparison of Measured and Analytical Results, Nozzle 53528, No Secondary Ports.....	30
14.	Illustration of CJTVC Operating Regions (No Secondary Ports).....	32
15.	Static Pressure Distribution, Nozzle 53528, No Secondary Ports.....	33
16.	Vectoring Performance, Nozzle 44022, Secondary Ports Located at 0.50" from Nozzle Throat.....	35
17.	Vectoring Performance, Nozzle 53528, Secondary Ports Located at 0.75" from Nozzle Throat.....	36
18.	Vectoring Performance, Nozzle 53530(?), Secondary Ports Located at 0.75" from Nozzle Throat.....	37
19.	Comparison of Vectoring Performance, Nozzle Pressure Ratio (P_p/P_{amb}) = 13.0.....	38

20. Vectoring Performance, Nozzle 54028, Secondary Ports Located at 1.00" from Nozzle Throat..... 39

21. Vectoring Performance, Nozzle 54523, Secondary Ports Located at 1.00" from Nozzle Throat..... 40

22. Thrust Vector Angle, Nozzle 44022, Secondary Ports Located at 0.50" from Nozzle Throat..... 43

23. Thrust Vector Angle, Nozzle 53528, Secondary Ports Located at 0.75" from Nozzle Throat..... 44

24. Thrust Vector Angle, Nozzle 53530(2), Secondary Ports Located at 0.75" from Nozzle Throat..... 45

25. Comparison of Thrust Vector Angle, Nozzle Pressure Ratio (P_p/P_{amb}) = 13.0 46

26. Effect of Exit Height on Vectoring Performance, Nozzle 53530, Nozzle Pressure Ratio (P_p/P_{amb}) = 11.0..... 48

27. Effect of Exit Height on Vectoring Performance, Nozzle 54028, Nozzle Pressure Ratio (P_p/P_{amb}) = 11.0..... 49

28. Effect of Port Location on Vectoring Performance, Nozzle 53530, Nozzle Pressure Ratio (P_p/P_{amb}) = 11.0..... 50

29. Illustration of CJTVC Vectoring Modes..... 52

30. Effect of Port Location on Vectoring Performance, Nozzle 54523, Nozzle Pressure Ratio (P_p/P_{amb}) = 11.0..... 53

31. Design Guidelines for 2-D CJTVC Nozzles (Talda[9])..... 55

32. Revised Design Guidelines for 2-D CJTVC Nozzles..... 56

33. Effect of Secondary Ports on Axial Efficiency, Nozzle 54523..... 59

34. Effect of Secondary Ports on Axial Efficiency, Nozzle 53528..... 60

35. Effect of Secondary Ports on Axial Efficiency, Nozzle 44022..... 61

36. Static Pressure Distribution, Nozzle 53528, No Secondary Ports..... 77

37. Nozzle Static Pressure, Nozzle 53528, No Secondary Ports..... 78

38. Static Pressure Distribution, Nozzle 53528, No Secondary Ports..... 80

39. Pressure Gradient Downstream of Separation Point..... 81

40. Flow Separation Point, Comparison of Measured and Analytical Results, Nozzle 44020, No Secondary Ports..... 82

41. Flow Separation Point, Comparison of Measured and Analytical Results, Nozzle 44022, No Secondary Ports..... 83

42. Flow Separation Point, Comparison of Measured and Analytical Results, Nozzle 53531, No Secondary Ports..... 84

43. Flow Separation Point, Comparison of Measured and Analytical Results, Nozzle 54028, No Secondary Ports..... 85

44. Flow Separation Point, Comparison of Measured and Analytical Results, Nozzle 54523, No Secondary Ports..... 86

List of Tables

Table		Page
I.	Values for 2-D CJTVC Design Variables.....	10
II.	Estimation of the Maximum Uncertainties of the Calibration Data Relative to the Linear "Least Squares" Curve Fit.....	68

List of Symbols

Symbol	Description	Units
a_e	Speed of Sound at the Nozzle Exit	ft/sec
a_t	Speed of Sound at the Nozzle Throat	ft/sec
A_e	Exit Area	in^2
A_s	Nozzle Area at the Point of Flow Separation	in^2
A_{si}	Secondary Injection Port Area	in^2
A_t	Throat Area	in^2
F_s	Side Force	lb_f
g_c	Constant of Proportionality	lb_m-ft/lb_f-sec^2
H_e	Exit Height	in
H_t	Throat Height	in
k	Specific Heat Ratio	--
L	Nozzle Length	in
$\dot{m}$	Mass Flow Rate	lb_m/sec
M_e	Nozzle Exit Mach Number	--
n	Velocity Profile Power Law Index	--
NPR	Nozzle Pressure Ratio (P_p/P_{amb})	--
P_{amb}	Ambient Pressure	psia
P_e	Nozzle Exit Pressure	psia
P_p	Primary Pressure	psia
P_{recirc}	Average Pressure Downstream of the Separation Point	psia
P_{si}	Secondary Pressure	psia
R_1	Gas Constant	psia-ft^3/lb_m-^oR
R_2	Gas Constant	ft^2/sec^2-^oR
T_p	Primary Temperature	^oR

V_e	Nozzle Exit Velocity	ft/sec
X_s	Axial Distance from Nozzle Throat to the Flow Separation Point	in
X_{si}	Axial Distance from Nozzle Throat to the Secondary Injection Port	in
δ	Nozzle Divergence Angle	deg
θ	Nozzle Exit Angle	deg
ρ_t	Density	lb_m/ft^3

Abstract

An experimental study of the axial and vectoring performance of two-dimensional (2-D) confined jet thrust vector control (CJTVC) nozzles was performed. The effects of adding secondary injection ports and changing exit height and secondary injection port location were studied on several 2-D CJTVC nozzles. The axial and vectoring performance results for these nozzles were measured over a range of pressure ratios. An analytical method for predicting flow separation was found to be applicable to these nozzles. Guidelines for designing 2-D CJTVC nozzles, that can be vectored using secondary injection, were established. Recommendations for further study are made.

EXPERIMENTAL EVALUATION OF DESIGN VARIABLES FOR TWO-DIMENSIONAL CONFINED JET THRUST VECTOR CONTROL NOZZLES

I. Introduction

Background

The incorporation of multi-axis thrust vectoring exhaust nozzles into future weapon systems can provide significantly enhanced performance and maneuverability. Currently, most thrust vectoring exhaust nozzles use various mechanical methods to provide vectoring. This can result in significant penalties in terms of weight, complexity and cost. To reduce these penalties, innovative thrust vectoring concepts are required.

One class of nozzles that can provide thrust vectoring, while reducing weight and complexity, are referred to as secondary injection thrust vector control (SITVC) nozzles. These nozzles use secondary fluid injection to produce vectoring, thereby eliminating the need for movable flaps and complex actuation systems. Two SITVC concepts that have been studied previously are boundary layer thrust vector control (BLTVC) and confined jet thrust vector control (CJTVC).

The BLTVC concept, studied by Carroll and Cox[1] and Fitzgerald and Kampe[3], uses a conventional converging-

diverging (C-D) nozzle designed such that the flow separates from the nozzle wall prior to reaching the exit (Figure 1). Secondary injection ports are located in the divergent portion of the nozzle so that ambient or pressurized air can be allowed to enter the nozzle. In the axial mode (Figure 1(a)), the secondary ports are all closed and the nozzle operates like an overexpanded C-D nozzle. Vectoring is achieved by opening one or more secondary ports and allowing either ambient or pressurized air to enter the nozzle. The secondary fluid injection causes a pressure imbalance in the nozzle divergent section and forces the primary stream to attach to the wall opposite of the opened secondary port(s) (Figure 1(b)).

The CJTVC concept, developed by Fitzgerald and Kampe[3], is a derivative of the BLTVC concept and operates on the same basic principles. The main difference between BLTVC and CJTVC is that the CJTVC nozzle has a reconvergent section added to the nozzle exit (Figure 2). The reconvergent section provides a larger exit angle for the primary stream and also tends to isolate the recirculation zone from the ambient pressure. This allows the CJTVC nozzles to provide a larger vector force, especially at high altitudes, over what can be achieved with BLTVC nozzles. However, this also requires that a source of high pressure air be available in order to produce vectoring.

The operating modes for the CJTVC nozzles are shown in Figure 2. In the axial mode (Figure 2(a)), the CJTVC

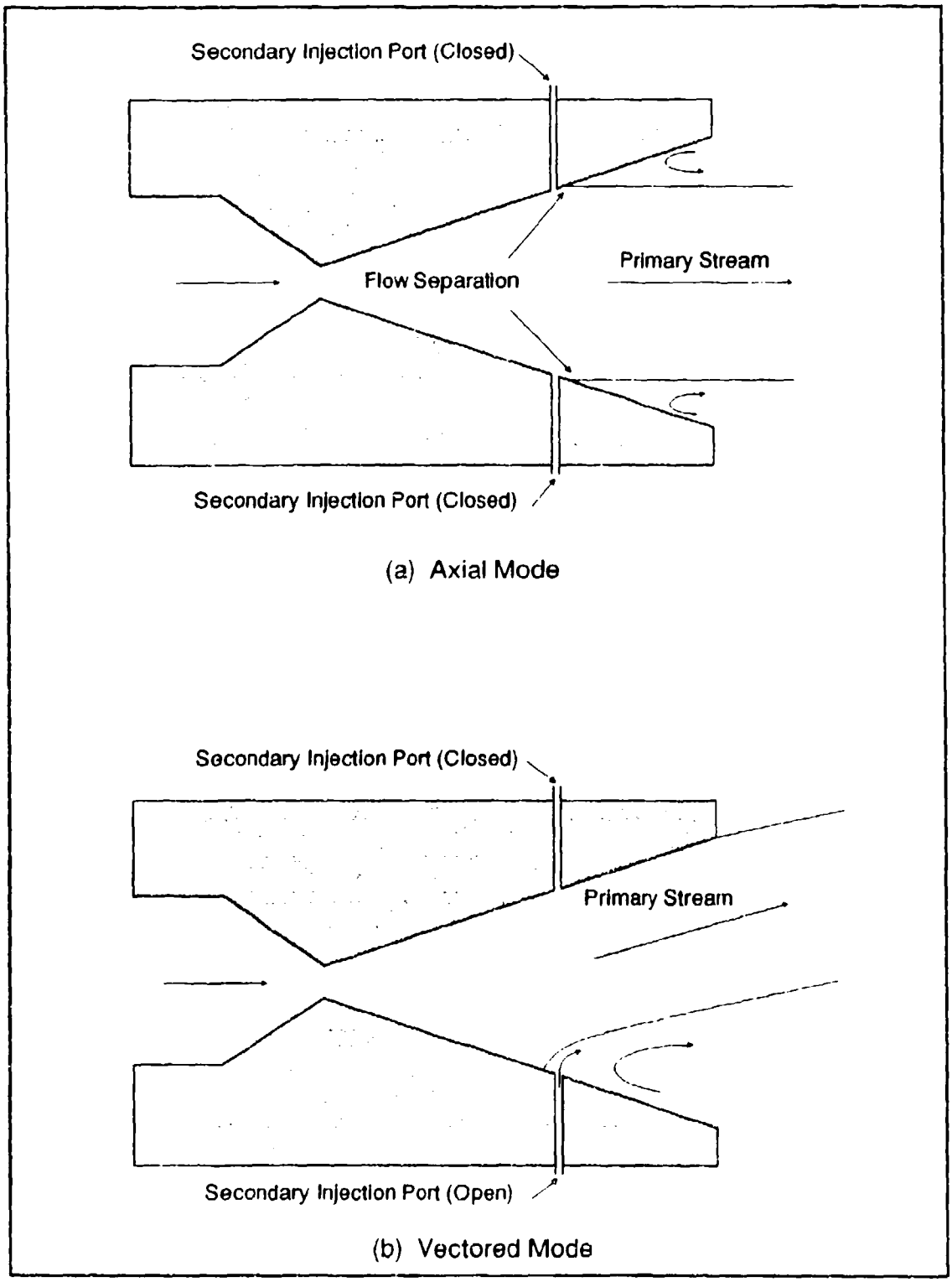

Figure 1 Illustration of BLTVC Operating Modes

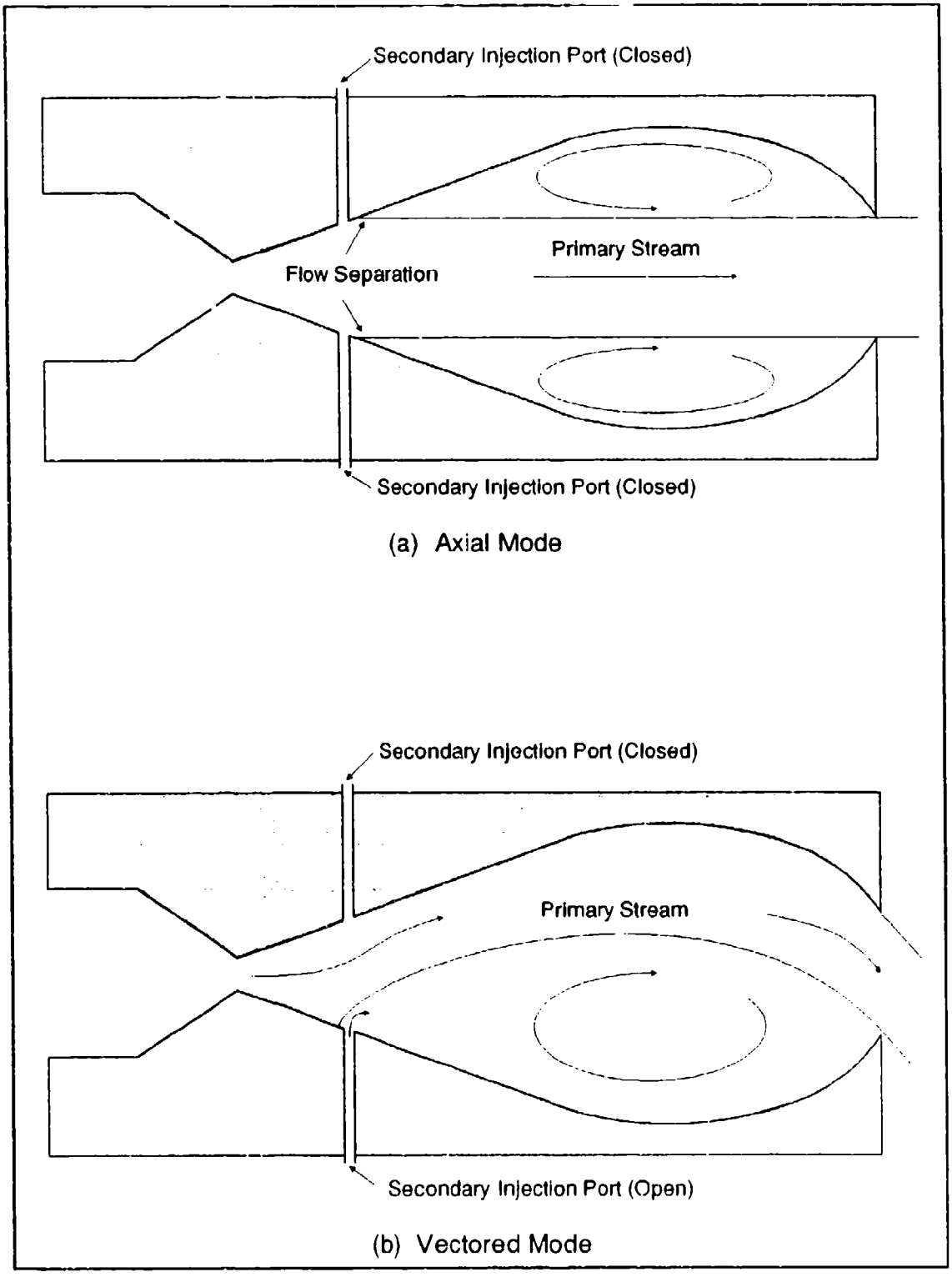

Figure 2 Illustration of CJTVC Operating Modes

nozzle operates in the same manner as the BLTVC nozzles. The only difference is that the recirculation zone in the CJTVC nozzle is isolated from the ambient conditions. During the vectored mode (Figure 2(b)), flow is injected through the secondary port(s). This secondary flow forces the primary stream to attach to the wall opposite of the opened port(s).

An experimental study of an axisymmetric CJTVC nozzle, conducted by Porzio and Franke[6], showed that thrust vector angles in excess of 20 degrees are possible with these nozzles. However, the axial thrust was only about 60-65% of the ideal thrust. Additional testing of axisymmetric CJTVC nozzles were also conducted by Lambert and Franke[5] and Friddell and Franke[4]. The results of these studies showed that CJTVC nozzles are competitive alternatives to BLTVC nozzles.

Cates[2] expanded on the axisymmetric work and constructed several two-dimensional (2-D) CJTVC nozzles. These 2-D nozzles allowed for visualization of the nozzle internal flow field during both axial and vectored conditions. Results of Cates' study showed that only one of the nine nozzles tested operated as a CJTVC nozzle, using secondary injection. Results for the other nozzles showed that the flow was vectored and stable over the entire range of primary pressures tested. Stability was defined as the flow being either vectored or axial with no significant force fluctuations. Additional results showed that both the axial and vectoring performance of 2-D CJTVC nozzles, as well as

the flow separation point, were functions of the nozzle exit height.

Talda[9] also investigated 2-D CJTVC nozzles by studying the effect of nozzle length, exit height and secondary port area and shape on the nozzle axial and vectoring performance. In addition, Talda also modified the contour of the nozzle divergent section so that the primary jet would follow the contour during vectored conditions. The results of Talda's tests showed that only two of the five nozzles tested could be operated as CJTVC nozzles. Results for the other nozzles showed that the flow was either stable in the axial position or unstable throughout the entire operating range. Additional results showed that there is a minimum secondary stream momentum and secondary port area required for vectoring. The secondary stream momentum was defined as the product of the secondary stream injector velocity and the secondary mass flow. The results also showed that both the side force and vector angle were functions of the secondary-to-primary pressure ratio, P_{si}/P_p.

Based on these results Talda suggested that one of the most critical parameters in designing a 2-D CJTVC nozzle was the nozzle length divided by the height of the exit. Therefore, in order to fully explore the potential benefits of 2-D CJTVC nozzles, it was evident that additional testing was required.

Objective

The first objective of this study was to expand the database for two-dimensional CJTVC nozzles by studying the effect of nozzle length, throat height, exit height and secondary port location on the steady-state axial and vectoring performance of these nozzles. The second objective was to develop a set of guidelines for the design of 2-D CJTVC nozzles.

Approach

To achieve the stated objectives, eight 2-D CJTVC nozzles were fabricated with various throat heights, exit heights and lengths. Each nozzle was then tested over a range of nozzle pressure ratios (P_p/P_{amb}) from 6 to 16, without secondary ports, to identify any instabilities in the nozzles, establish baseline performance and to determine the flow separation point. Secondary ports were then added to several of the nozzles and tests were conducted to determine the vectoring ability and performance of these nozzles. Additional tests were conducted on two nozzles to determine the effect of port location on axial and vectoring performance. The effect of reducing exit height was also studied on two of the nozzles.

II. EXPERIMENTAL APPARATUS

Nozzle Design

The results of Talda's[9] study showed that only two of the nozzles tested could be operated as a CJTVC nozzle. Talda explained that the ratio of nozzle length to exit height appeared to be the critical parameter in determining the vectoring ability of the nozzles. Based on these results, the nozzles fabricated for this study used the design guidelines that were suggested by Talda[9]. Figure 3 shows an illustration of the design variables for the nozzles used in this study. Values for each of the design variables and an explanation of the numbering system for the nozzles are provided in Table I. Static pressure taps were located along the nozzle walls to determine the wall pressure distribution and flow separation point. The pressure taps for nozzles 44020, 44022 and 44517 were located at 1/4", 1/2", 3/4", 1", 1 1/4", 1.8", 2.4" and 3", from the nozzle throat, on one half of the nozzle and at 1", 1.8", 2.4" and 3" on the other half. The pressure taps for the remaining nozzles were located at 1/4", 1/2", 3/4", 1", 1 1/4", 2 1/4", 3", 3 3/4", from the nozzle throat, on one half of the nozzle and at 1", 2 1/4", 3" and 3 3/4" on the other half.

Nozzle Assembly

The nozzle assembly (Figure 4) consisted of three sections: 1) The aluminum mounting bracket, 2) The plastic sidewalls, and 3) the plastic nozzles. The mounting bracket

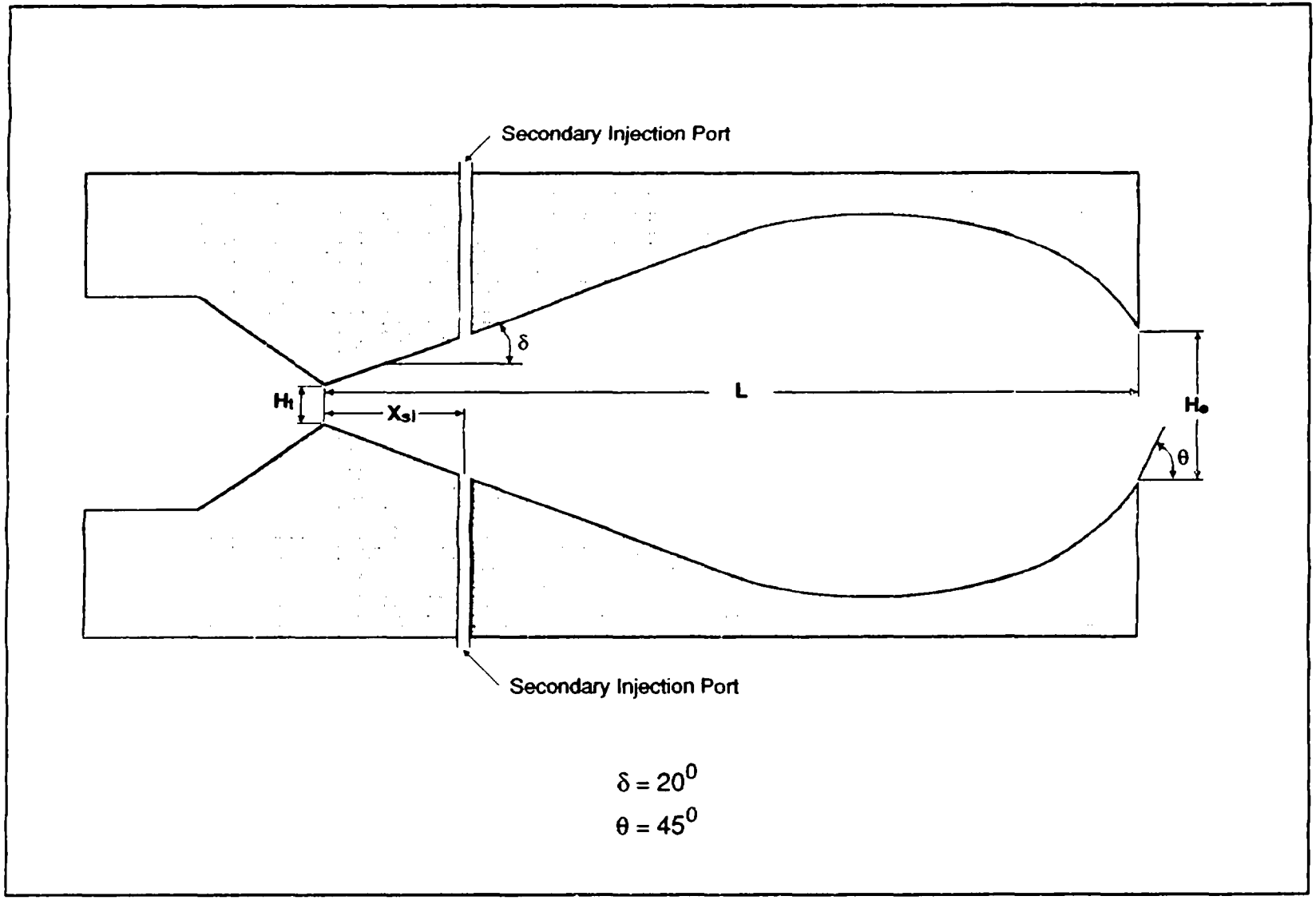

Figure 3 CJTVC Design Variables

Table I Values for 2-D CJTVC Design Variables

Nozzle	Length (L) (in)	Expansion Ratio (He/Ht)	Throat Height (in)	X_{sl} (in)	A_{sl}/A_t
44020	4.0	4.0	0.20	0.75	0.22
44022	4.0	4.0	0.22	0.50	0.21
44517	4.0	4.5	0.17	-	-
53528	5.0	3.5	0.28	0.75	0.21
53530	5.0	3.5	0.30	0.75	0.17*
53530(2)	5.0	3.23	0.30	0.75	0.17*
53530(3)	5.0	3.5	0.30	1.25	0.17*
53531	5.0	3.5	0.31	-	-
54028	5.0	4.0	0.28	1.00	0.20
54028(2)	5.0	3.57	0.28	1.00	0.20
54523	5.0	4.5	0.23	1.00	0.19
54523(2)	5.0	4.5	0.23	1.25	0.19

* This was due to a manufacturing error, the design value was 0.20

Example of Nozzle Numbering System

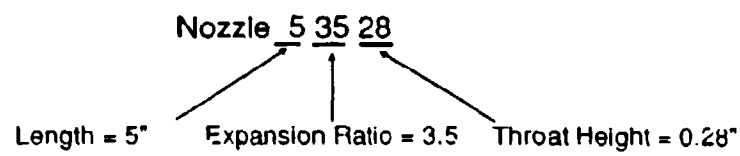

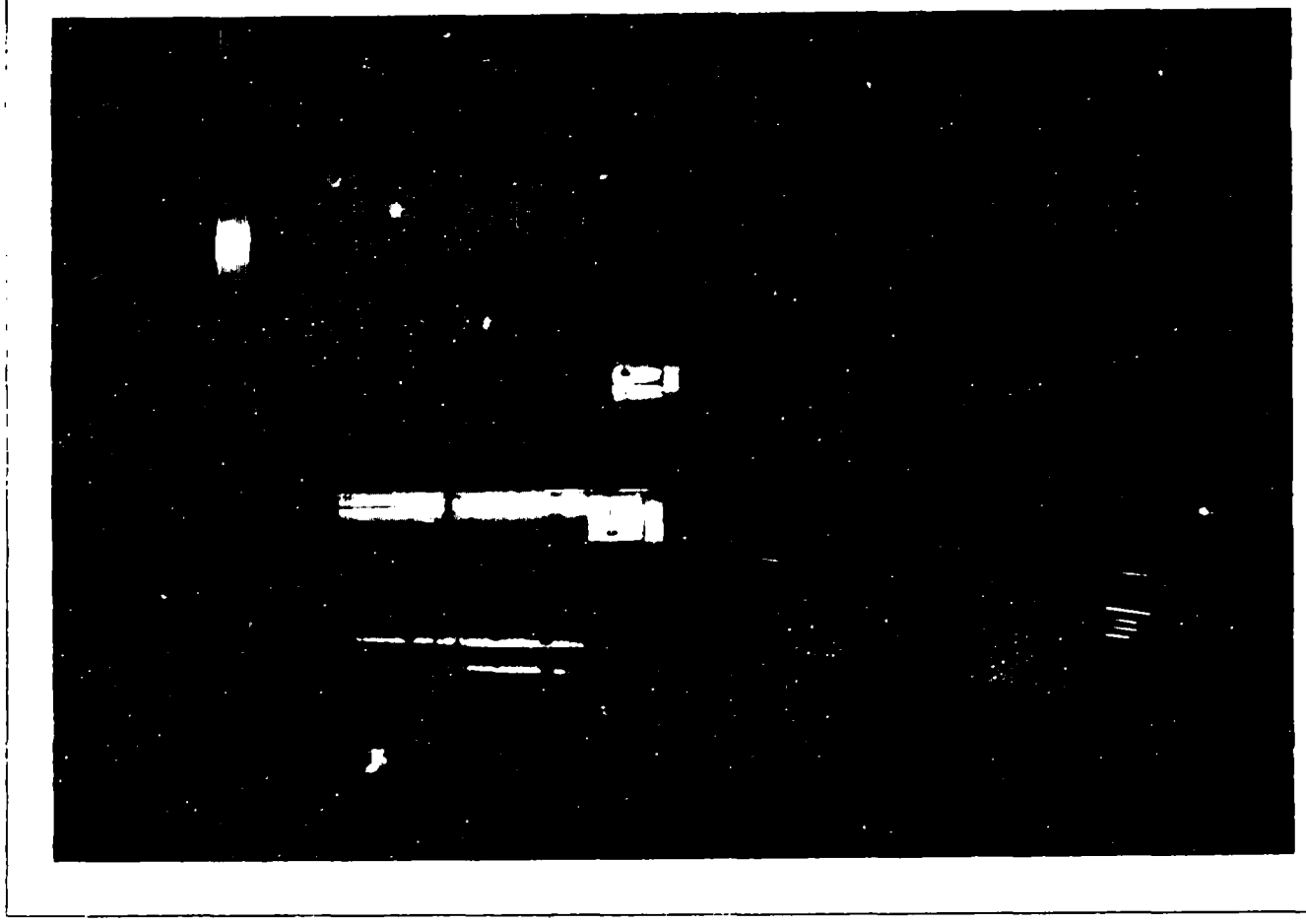

Figure 4. Photograph of Nozzle Test Assembly

was the same one that was used by Talda[9]. The sidewalls were constructed of 3/4" clear plastic, to allow for the use of flow visualization. Each nozzle consisted of two halves, identical in shape, and were fabricated from 3/4" plastic. The sidewalls were bolted to the mounting bracket and the nozzle halves were then placed between the sidewalls and pins were inserted to prevent any motion during testing. Bolts were used around the perimeter of the bracket to ensure proper sealing and the entire assembly was then bolted to the primary plenum.

Test Stand

A photograph of the test stand is shown in Figure 5, and a schematic of the test stand is shown in Figure 6. The stand consisted of a steel frame that supports the primary air supply pipe and the primary plenum. The primary air supply pipe had a two-degree of freedom pivot to eliminate the transfer of any axial or side loads to the frame. The primary plenum was attached to the primary air supply pipe and also to the force balance, which was anchored to the floor of the test cell. Secondary air for the nozzle was provided through a manifold attached to the primary plenum. Secondary air is supplied to the nozzle by flexible tubing and solenoid valves that are attached to the manifold.

Primary and Secondary Flow System

Controls for operating the primary and secondary flows were located in an enclosed control room. The primary

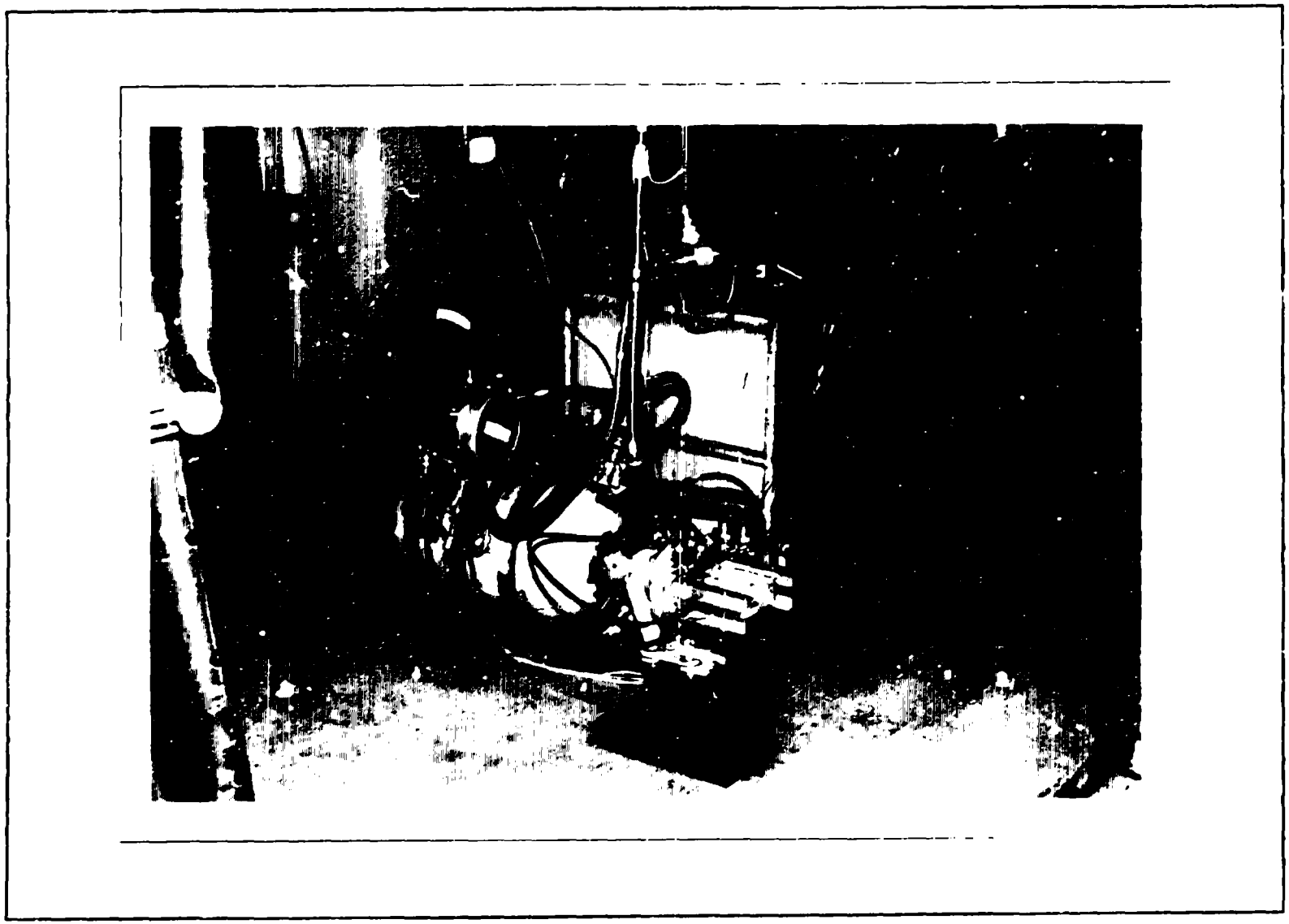

Figure 5. Photograph of Test Stand

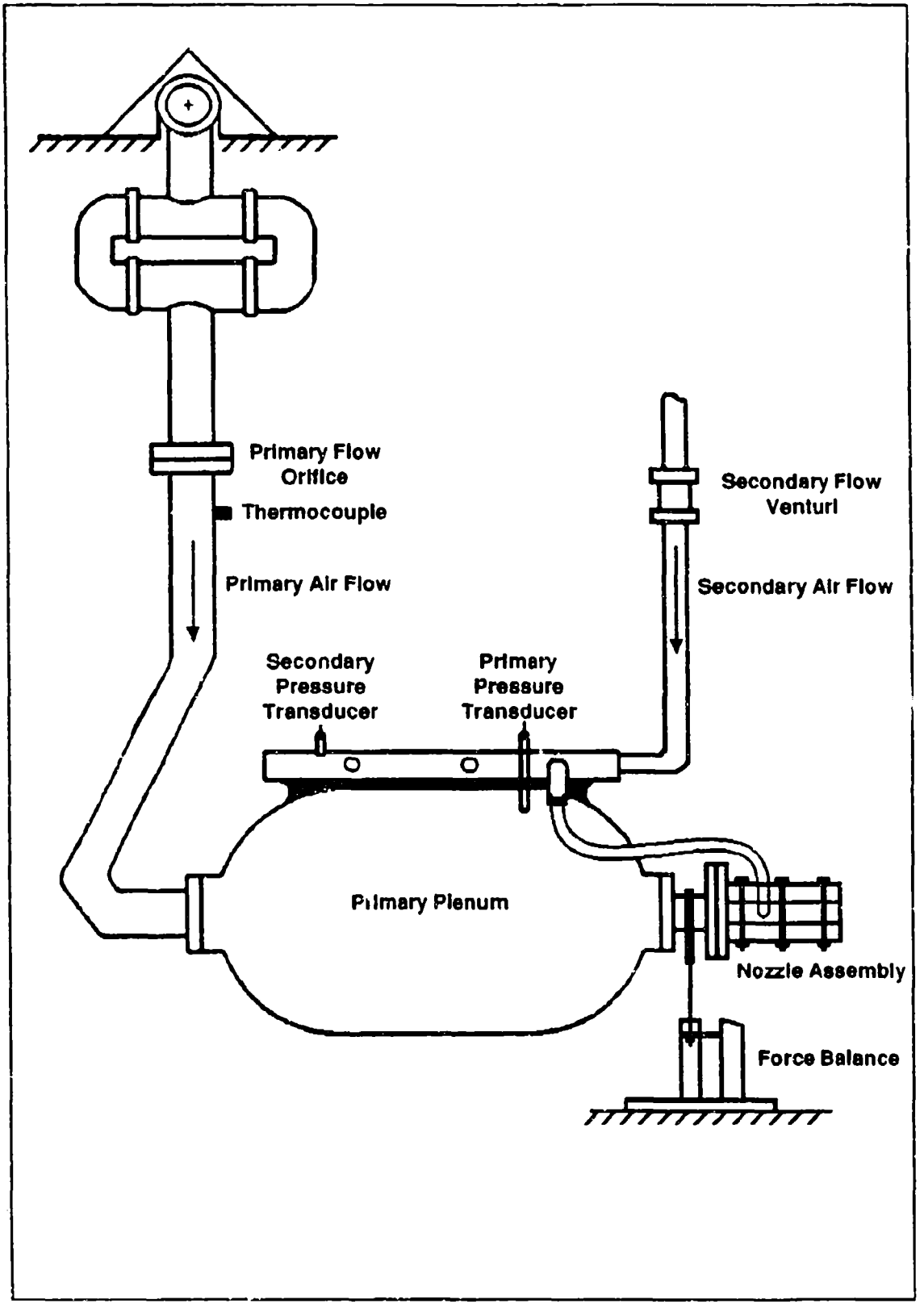

Figure 6 Schematic of Test Stand

flow was controlled by a dual dome valve system that was operated from within the control room. The secondary air was controlled by a hand valve located in the control room and a remotely controlled solenoid valve attached to the primary plenum.

Force Measurements

The axial and side forces were measured using a force balance (Figure 7) that was bolted to the floor of the test cell. The force balance consisted of a support base that was bolted to the floor of the test cell and two perpendicular links that were connected by a yoke to the nozzle assembly. The forces were measured by strain gauges located between the links and the support base. Calibration of the force balance was accomplished with weights suspended by a cable and pulley system attached to the nozzle assembly. An uncertainty analysis for the force balance is provided in Appendix A. The axial and side forces were calibrated separately. However, both side force and axial force were measured for each set of calibrations in order to identify any coupling between the axial and side force. Results of the calibration showed that there was a coupling effect between the side force and the axial force. The side/axial force coupling was a result of the side and axial links on the force balance not being exactly perpendicular. The measured results for all the nozzles were corrected for this coupling effect.

Figure 7. Photograph of Force Balance

Static Pressure Measurements

Twelve static pressure transducers were used to measure the wall pressure distribution during each test run. Flexible tubing was used to connect the pressure taps in the nozzle to the pressure transducers. These transducers had a pressure range of +/- 50 psid and were located on a cart near the test stand. The distance between the pressure taps and the transducers was about four feet. The outputs from the transducers were then connected to the data acquisition system. All the transducers were calibrated, using a deadweight tester, prior to testing and an uncertainty analysis for these transducers is provided in Appendix A.

Mass Flow Measurement

The primary mass flow was measured using a thin plate orifice, primary pressure transducer and a differential pressure transducer. The orifice and differential pressure transducer were located on the primary supply pipe, upstream of the primary plenum and the primary pressure transducer was located on the primary plenum (Figure 6). Secondary mass flow was measured by a Venturi, secondary pressure transducer and a differential pressure transducer. The Venturi and the differential pressure transducer were located upstream of the secondary supply manifold and the secondary pressure transducer was located on the secondary supply manifold (Figure 6).

Temperature Measurement

The primary supply air temperature was measured by an

chromel-alumel thermocouple, inserted into to the primary supply pipe and located slightly downstream of the orifice (Figure 6). The secondary air temperature was assumed to be the same as that of the primary flow.

Flow Visualization

A schlieren system was setup to allow for visualization of the nozzle internal flow field during both axial and vectored conditions. The setup consisted of two spherical mirrors, a knife edge and a zirconium lamp. The zirconium lamp produced a steady light source that allowed for video taping of the internal flow field. A review of the video tape revealed that although this allowed for visualization of the flow field dynamic behavior, the quality of the video was not very good.

Data Acquisition System

The data acquisition system consisted of a HP-85A computer that controlled a HP-3497A data scanner. Outputs from all the instrumentation, except for the thermocouple, were sampled by the data acquisition system and then transferred to the computer during each test condition. Temperature data was input to the computer manually for each test condition.

III. Experimental Procedure

The procedure for setting-up and collecting data for each test condition was as follows:

1. The data acquisition system was turned on and test control program was initialized. This program controls the data acquisition system, reads the zero values for each channel, records the values of each channel during the test condition, and performs the data reduction.

2. Ambient pressure and temperature were input to the computer.

3. The secondary manifold pressure was set to the desired pressure by the control valve in the control room, when required.

4. The primary pressure was then set to the desired pressure, using the dual dome valve system.

5. When the primary pressure had stabilized at the desired value for about 15 seconds, the data acquisition was started. During each run the data acquisition system sampled each channel (pressures and forces) and stored the results in the computer. During each test condition the data acquisition systems sampled all 18 data channels 15 times and the results for each channel were then averaged and stored in the computer. The duration of each test run lasted about one minute. (Note: all the measured data was for steady-state conditions.)

6. At the completion of each test condition, the

primary pressure was shut off from inside the control room and secondary pressure, when required, was also shut off.

7. Primary air temperature was then entered into the computer and a hard copy of the test results was printed.

IV. Results and Discussion

Baseline Results

All eight CJTVC nozzles were tested, without secondary injection ports, over a range of nozzle pressure ratios (NPR) from 6 to 16. The NPR was defined as the primary pressure divided by the ambient pressure, P_p/P_{amb}. The results of these tests were used to identify any inherent instabilities that might be present in the nozzles and to establish baseline nozzle performance. In addition, these tests were also used to determine the location of the flow separation, as a function of NPR, within the nozzles. Determination of the flow separation point is critical in order to properly locate the secondary ports.

Results from the baseline tests showed that all the nozzles, except for nozzle 44517, were stable and had no significant side force fluctuations over the entire range of NPRs tested. Stability was defined as the flow being either axial or vectored with no significant force fluctuations. Figure 8 shows typical side force fluctuations for nozzles 44517 and 44020. The results for nozzle 44020 are also typical of the measured responses for the remaining nozzles. No useful results were obtained for nozzle 44517 because of the unstable flow in this nozzle.

The axial efficiencies (measured thrust divided by ideal thrust) for these nozzles are shown in Figures 9 and 10.

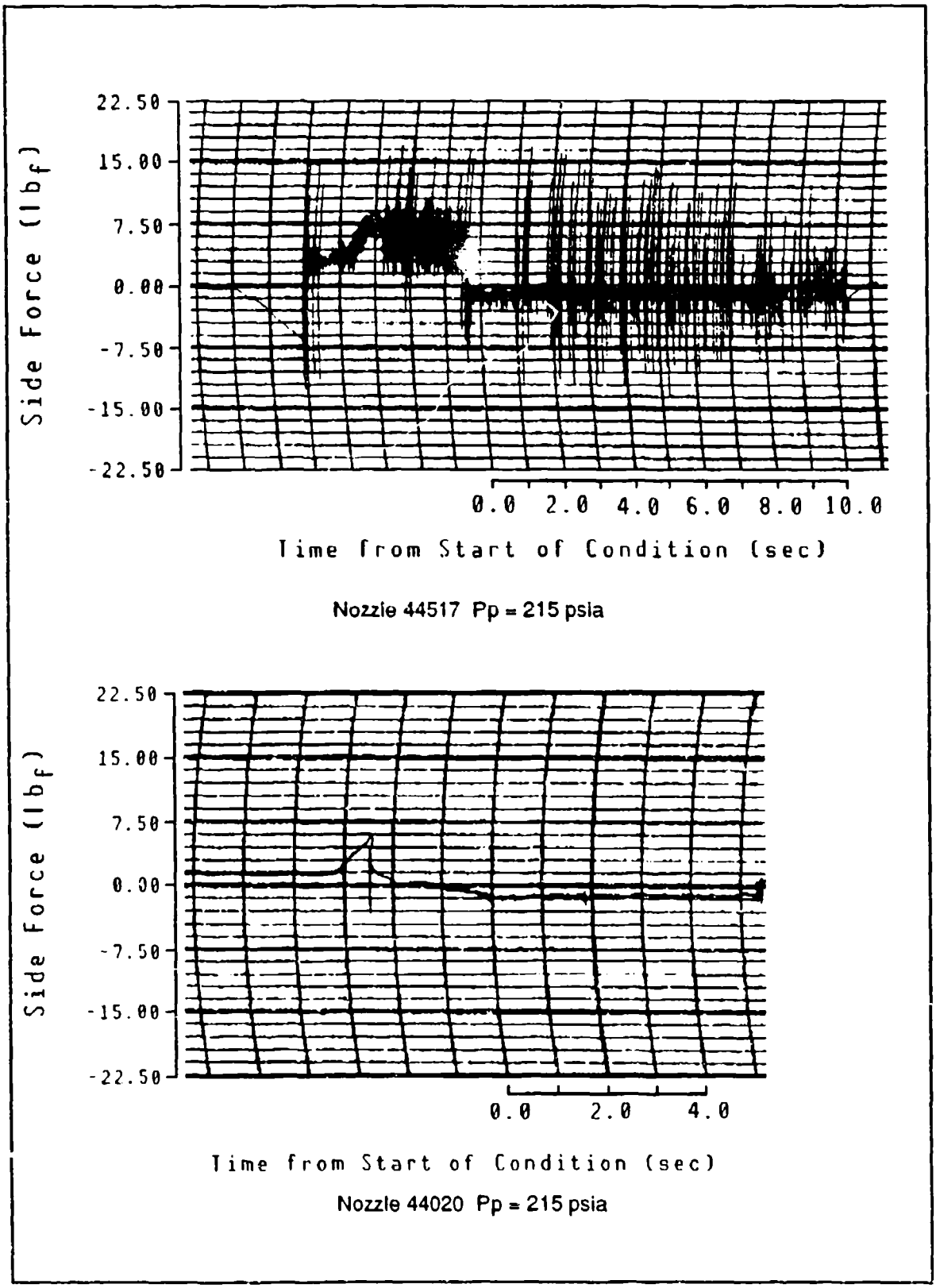

Figure 8 Nozzle Stability During Axial Tests, No Secondary Ports

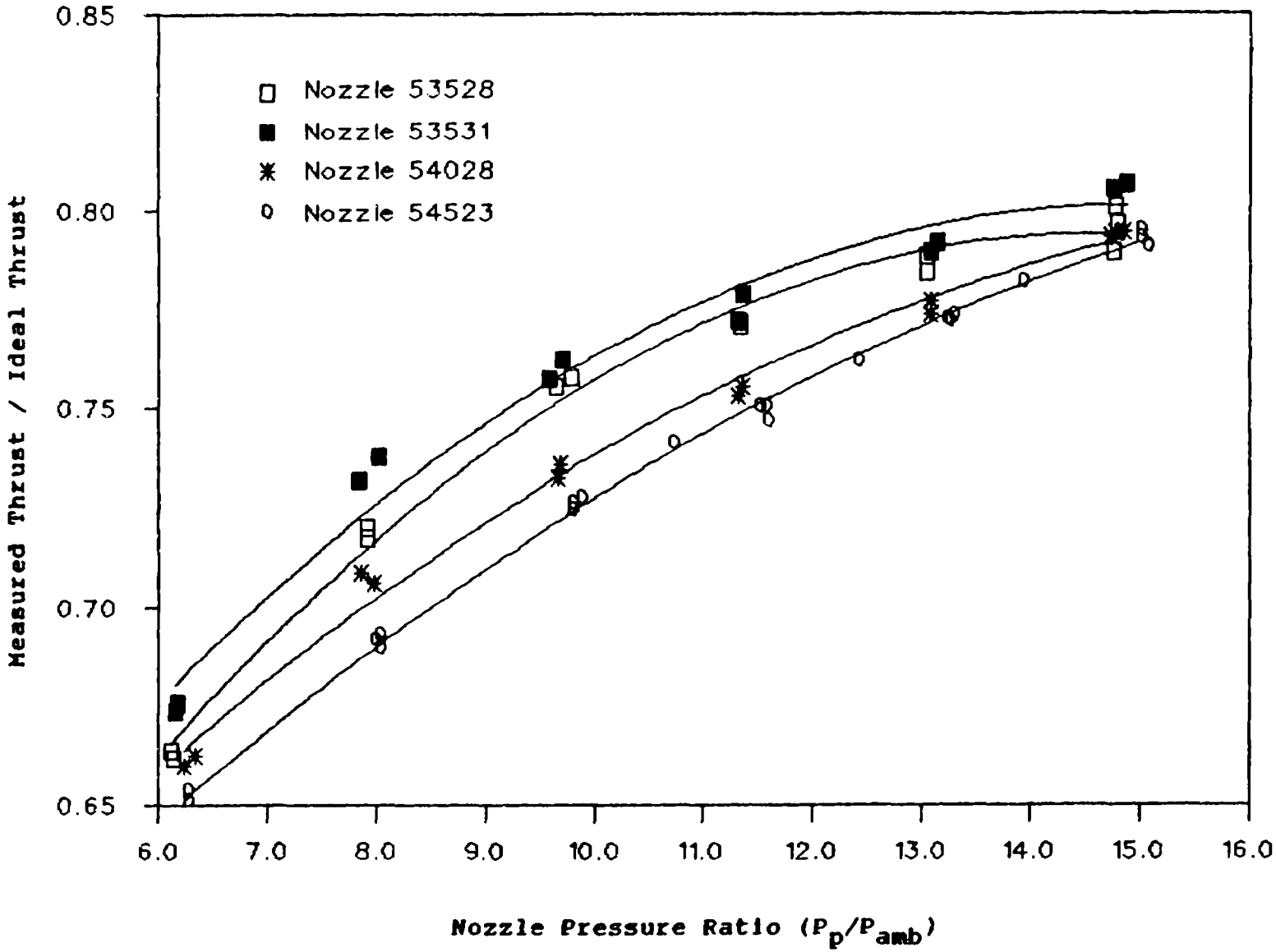

Figure 9. Nozzle Axial Efficiency, No Secondary Ports, Length = 5"

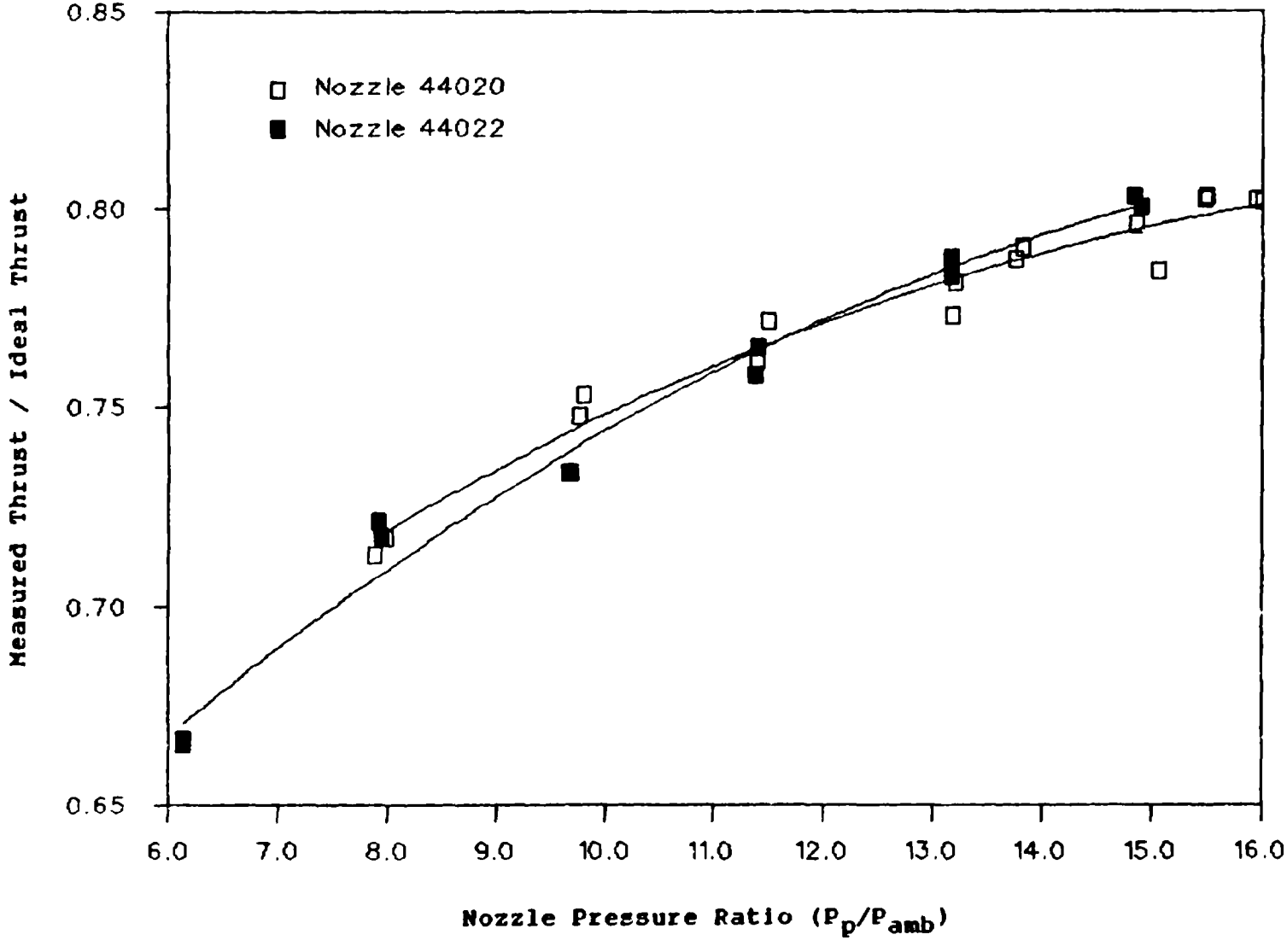

Figure 10. Nozzle Axial Efficiency, *No Secondary Ports, Length = 4"*

The ideal thrust for each nozzle was calculated by assuming one-dimensional, isentropic expansion through a conventional converging-diverging (C-D) nozzle. The C-D nozzle was assumed to have the same throat area as each of the nozzles tested and the flow was assumed to be fully-expanded (nozzle exit pressure equal to ambient pressure). The equations used to calculate the ideal thrust are provided in Appendix B. Results for nozzle 53530, without secondary ports, are not shown because the primary pressure transducer was inoperable during this test.

The results in Figures 9 and 10 show that the nozzle axial efficiency increases as the NPR was increased, similar to a conventional C-D nozzle, but their efficiencies are substantially lower than a C-D nozzle. This is due to the fact that CJTVC nozzles operate in an overexpanded condition. Figure 9 also shows that although the expansion ratio (H_e/H_t) has a has a small impact on nozzle performance, there is a noticeable effect on the slope of the efficiency curve. Figure 11 shows the results for nozzles 53528 and 54028. Notice that the efficiency for nozzle 53528 has leveled off at a NPR of about 14.0, while the efficiency of nozzle 54028 is still increasing. The reason for these differences will be discussed later in this section.

The location of the flow separation was determined by using two separate methods. The first was an analytical prediction method developed by Thompson[10]. This method was also used by Friddell and Franke[4] to study flow separation in

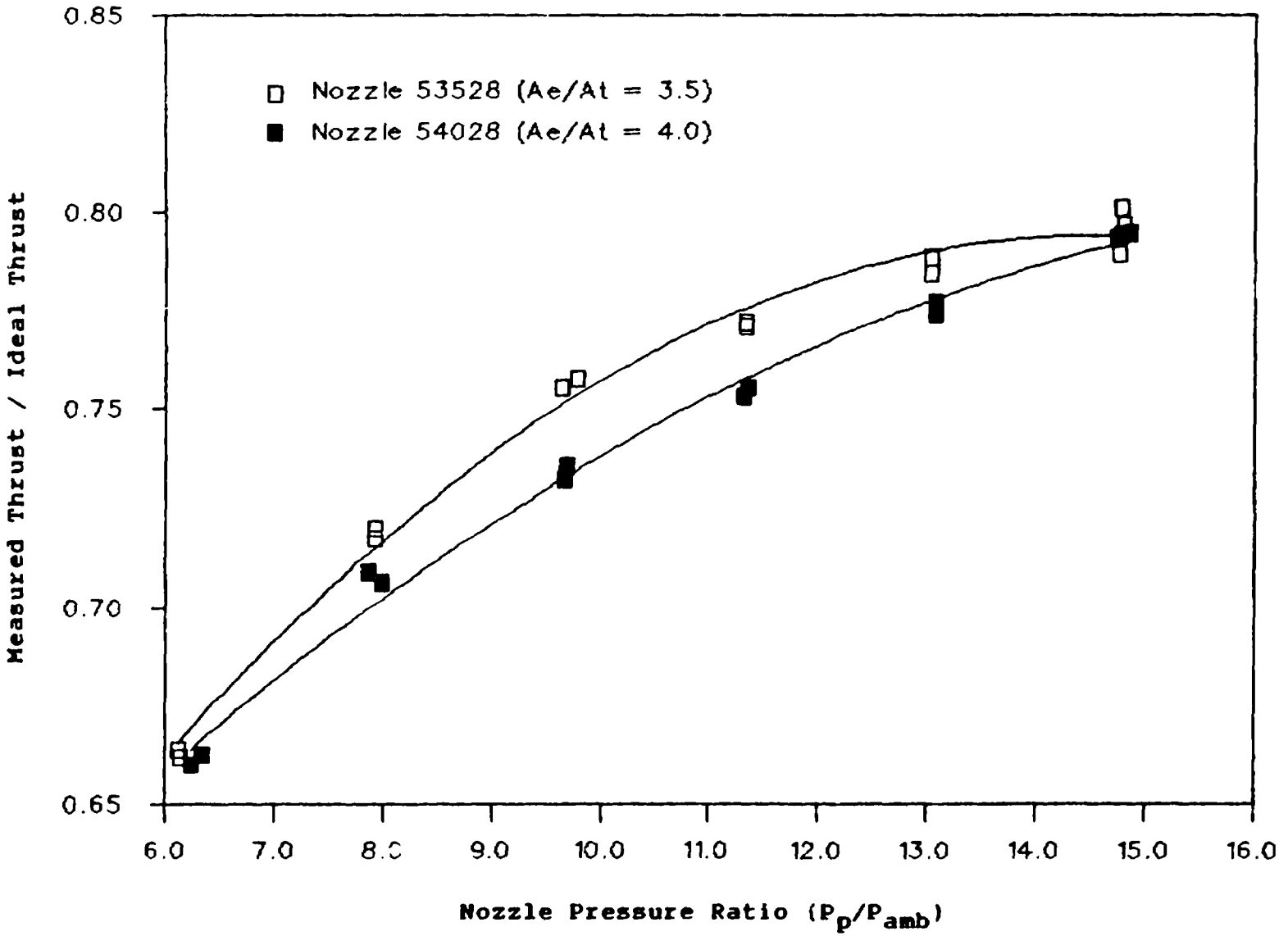

Figure 11. Effect of Expansion Ratio (A_e/A_t) on Nozzle Axial Efficiency, No Secondary Ports

axisymmetric CJTVC nozzles. Thompson developed this method by equating the boundary layer momentum to the applied back pressure and then derived an equation for the isentropic Mach number at separation, as a function of the NPR. However, when applying this method to CJTVC nozzles it is important to note that the definition of NPR needs to be modified. Figure 12 shows the typical nozzle static pressure distribution for the nozzles that were tested. The important thing to note is that the effective back pressure imposed on the boundary layer can be significantly different from the ambient pressure. Therefore, the NPR used in Thompson's method needs to be redefined as the primary pressure divided by the pressure in the recirculation region (P_p/P_{recirc}). The pressure in the recirculation region (P_{recirc}) was calculated as the average pressure measured downstream of the separation point on one half of the nozzle. The detailed equations and calculations for Thompson's method are provided in Appendix C. The results from Friddell and Franke's[4] study showed that this method can be used to accurately predict the flow separation point, as a function of primary pressure, in axisymmetric CJTVC nozzles.

The second method for determining the flow separation point consisted of using plots of the static pressure distribution within the nozzle (Figure 12). Figure 12 shows that the nozzle static pressure decreases as the area increases, in agreement with the isentropic flow relation, until separation occurs, at which point the pressure rises

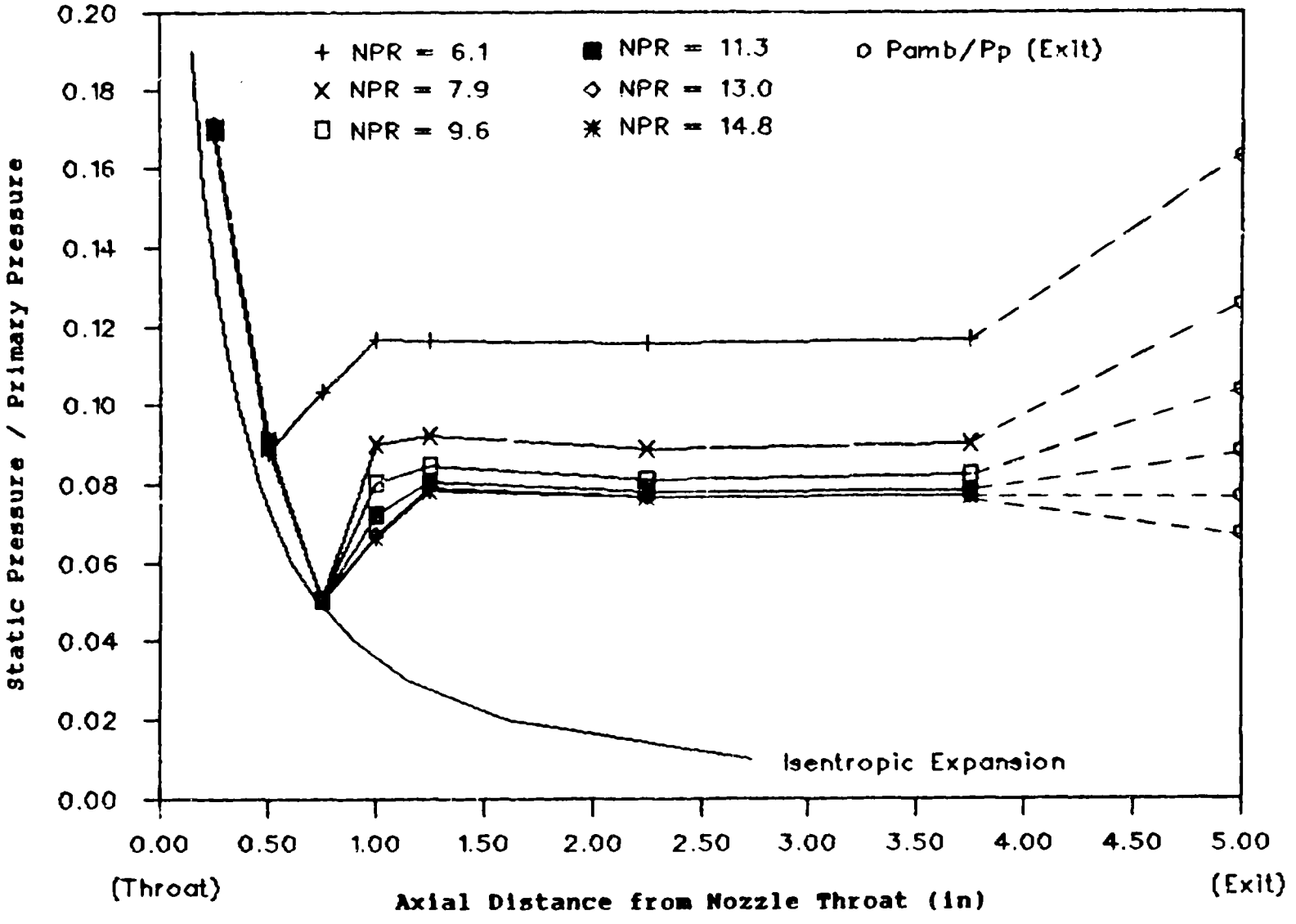

Figure 12. Static Pressure Distribution, Nozzle 53528, No Secondary Ports

rapidly to some constant value. The point at which the pressure begins to rise is defined as the separation point. However, the accuracy of this method is very dependent upon the spacing of the pressure taps. The results for the nozzles tested showed that the pressure taps were located too far apart to accurately determine the separation point. Therefore, a method of adjusting this data to improve its accuracy was established and is described in Appendix D.

The results of locating the flow separation point, using the two methods described above, are shown in Figures 13 and 40 to 44. The adjusted experimental data is meant to represent the minimum axial location of the flow separation, based upon the results of the method described in Appendix D. The dashed line represents a "best guess" for the maximum axial location of the flow separation and is also discussed in Appendix D.

Figures 13 and 40 to 44 show that the location of flow separation, defined by Thompson's[10] method, is within the range of uncertainty established by the measured data. This indicates that Thompson's method is applicable to 2-D CJTVC nozzles, provided that the correct nozzle pressure ratio is used. In addition, these figures show that the location of the flow separation is a non-linear function of NPR (P_p/P_{amb}).

Figure 13 shows that at low NPRs (6 to 8), the axial location of the separation point increases linearly as the NPR is increased. However, as the NPR is increased further,

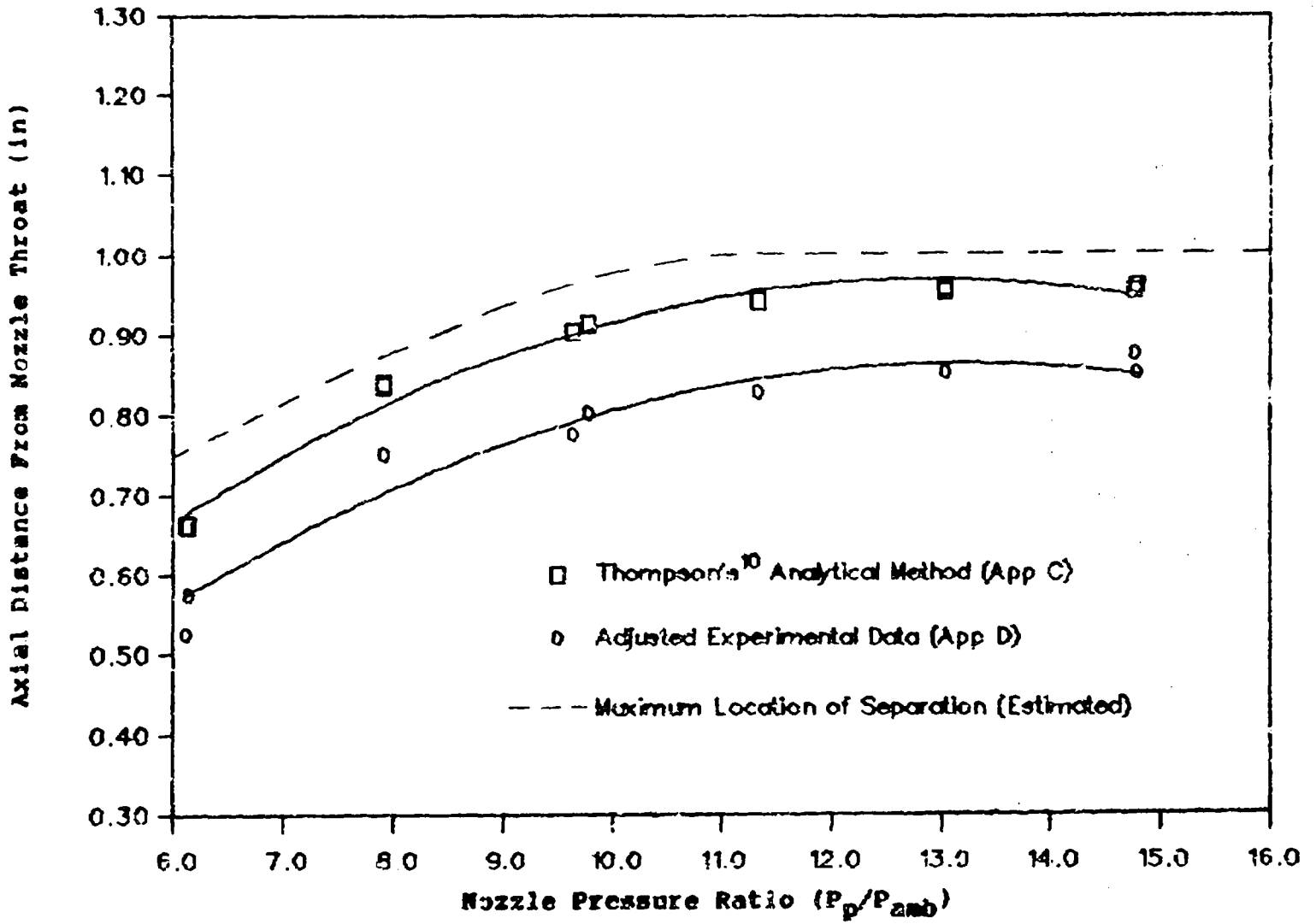

Figure 13. Flow Separation Point, Comparison of Measured and Analytical Results, Nozzle 53528, No Secondary Ports

the axial location of the separation point levels off at a point where the area at separation (A_s) is approximately equal to the exit area (A_e). The NPR at which this occurs is referred to as the design NPR. These results are also similar to those found by Friddell and Franke[4] for axisymmetric CJTVC nozzles.

The results in Figures 11 to 13 suggest that there are three distinct operating regions for CJTVC nozzles. The first region is illustrated in Figure 14(a). This shows that when the NPR is below the design NPR the flow separates at point where area ratio (A_s/A_e) is less than one and the pressure in the recirculation region is below ambient. This is also evident in the plot of the nozzle static pressure distribution (Figure 15, NPR=6.1). The second region is when the NPR is equal to the design NPR (Figure 14(b)). In this region the flow separates at a point where the area ratio (A_s/A_e) is approximately equal to one and pressure in the recirculation region is now equal to ambient (Figure 15, NPR=13.0). Finally, as the NPR is increased beyond the design NPR (Figure 14(c)), the flow separation point does not move but the pressure in the recirculation region becomes greater than ambient (Figure 15, NPR=14.8).

The operating regions described in Figure 14 are also useful in describing the axial performance results shown in Figures 9 to 11. At low NPRs, the flow separates at a point where the nozzle height at separation is less than the exit height (Figure 14(a)), which results in reduced axial

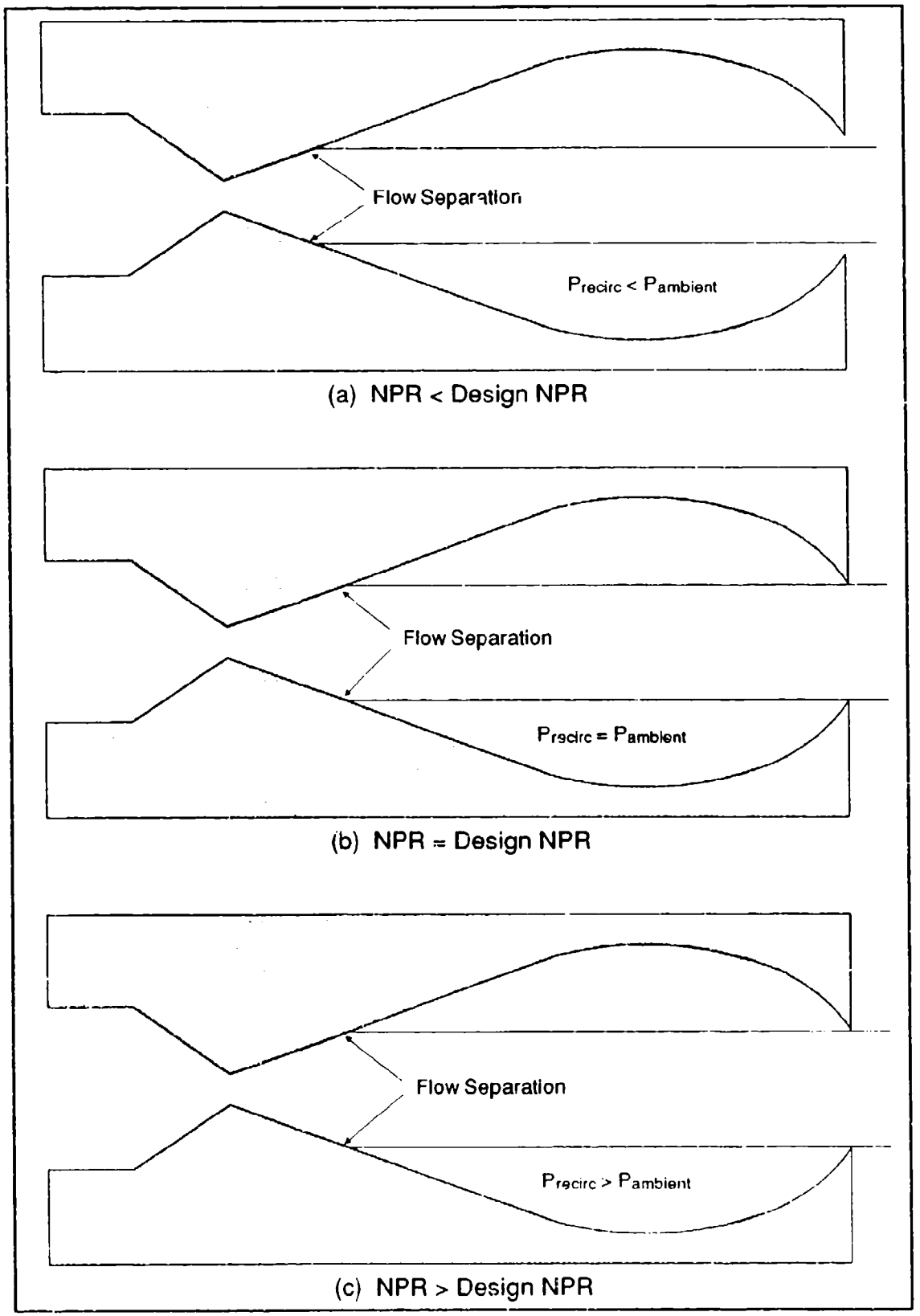

Figure 14 Illustration of CJTVC Operating Regions (No Secondary Ports)

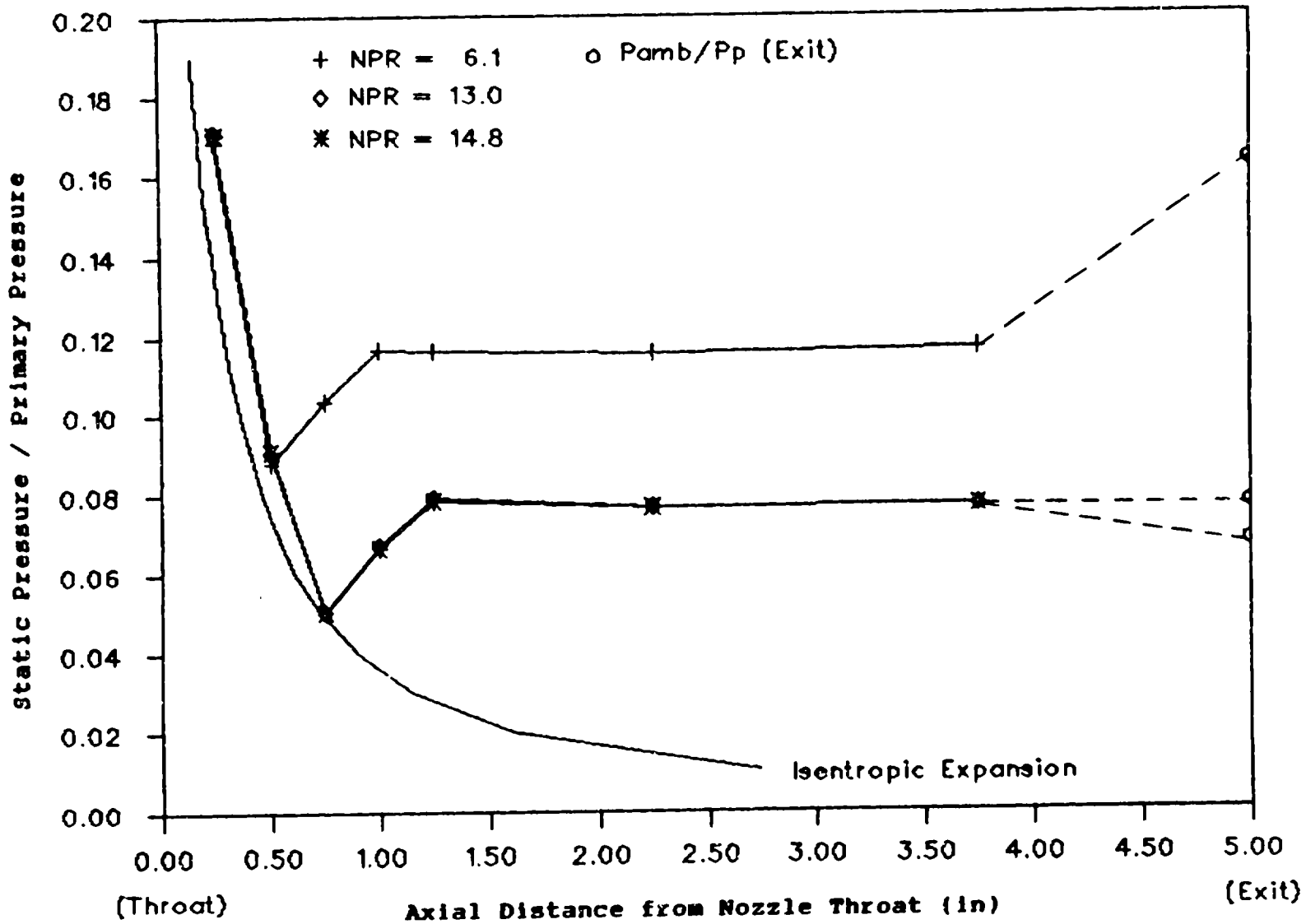

Figure 15. Static Pressure Distribution, Nozzle 53528, No Secondary Ports

efficiency. As the NPR is increased to the design NPR, the nozzle efficiency reaches a maximum and the pressure in the recirculation region is approximately equal to ambient. When the NPR exceeds the design NPR, the pressure in the recirculation region increases and tends to offset any thrust increase due to the increased NPR.

The results in Figure 11 also suggest that as the exit height is increased the design NPR is also increased. This is shown by noticing that the axial efficiency for nozzle 53528 has reached a maximum at the higher NPRs while the efficiency for nozzle 54028 is still increasing. These results are also consistent with the operating characteristics of an overexpanded C-D nozzle. That is, as the exit area is increased, the NPR required to fully expand the flow is also increased.

Vectoring Performance

The vectoring ability and performance of the nozzles were determined by adding secondary ports to all the nozzles, except 44517 and 53531, and testing them over a range of pressure ratios. The location and size of the secondary ports are shown in Table I. Results of the vectoring tests showed that 44022, 53528, and 53530 were the only nozzles that could be vectored using secondary injection. Results for these nozzles are shown in Figures 16 to 19 and the results for the remaining nozzles are shown in Figures 20 and 21. No results were obtained for nozzle 44020, with

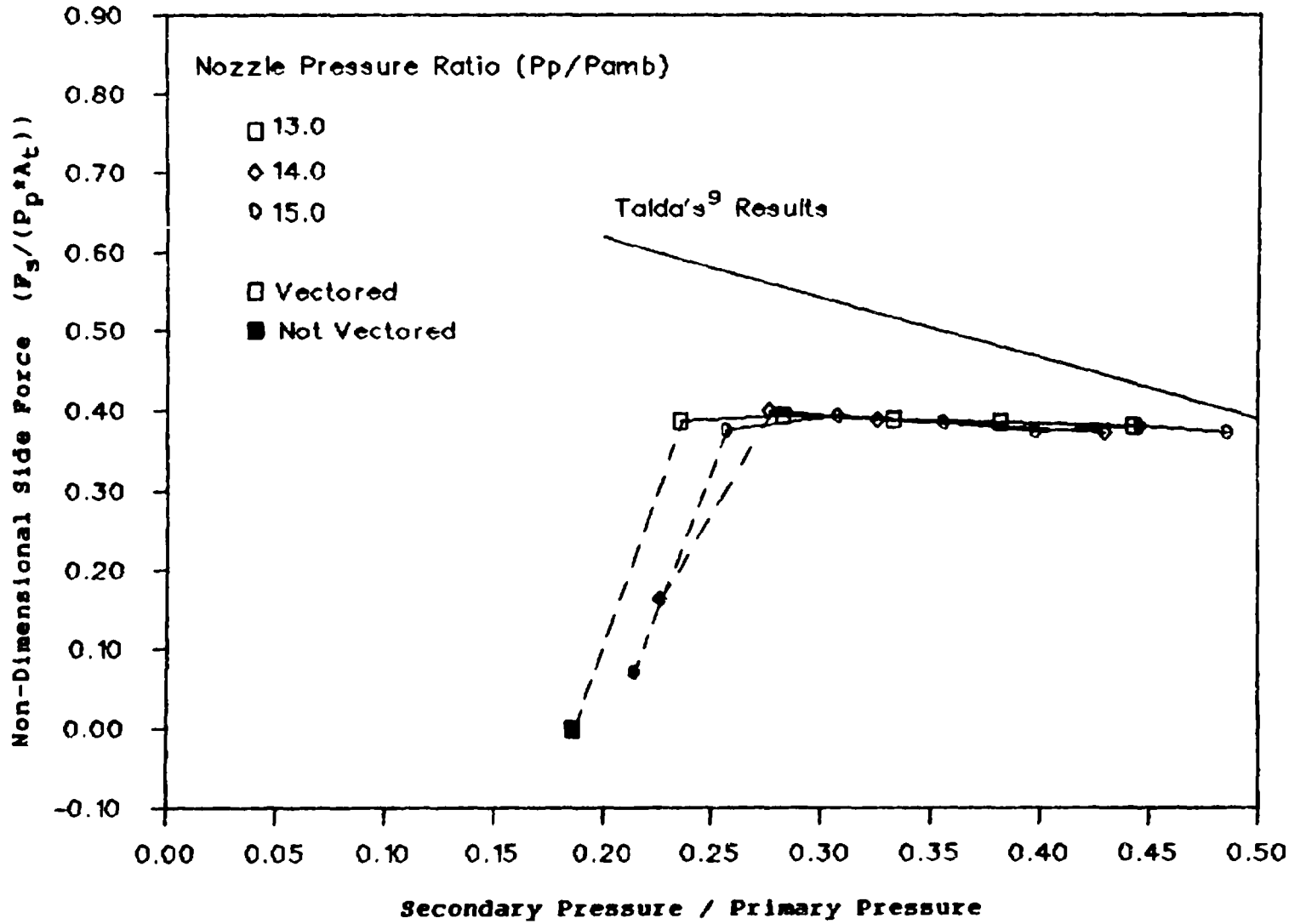

Figure 16. Vectoring Performance, Nozzle 44022, Secondary Ports Located at 0.50" from Nozzle Throat

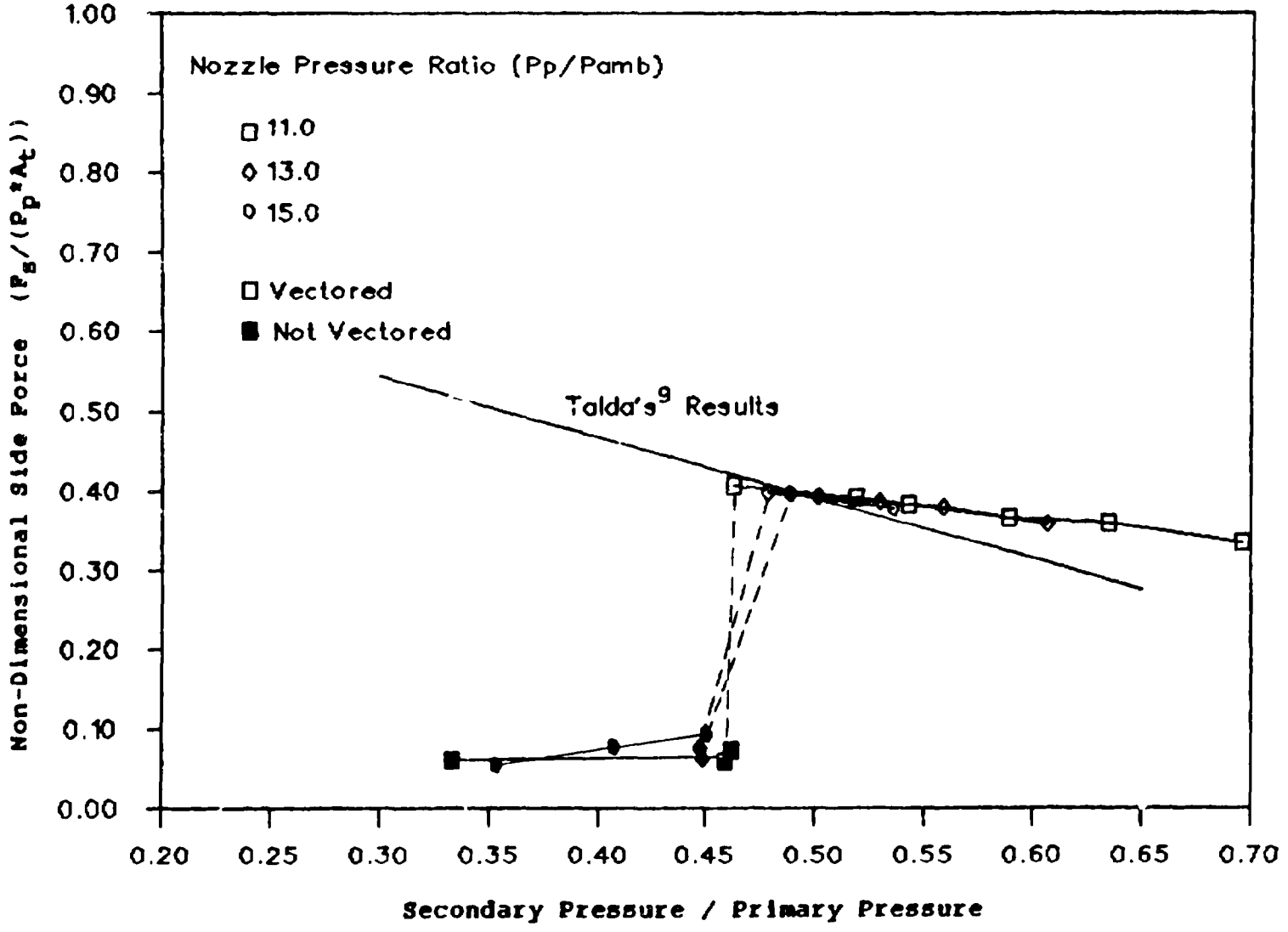

Figure 17. Vectoring Performance, Nozzle 53528, Secondary Ports Located at 0.75" from Nozzle Throat

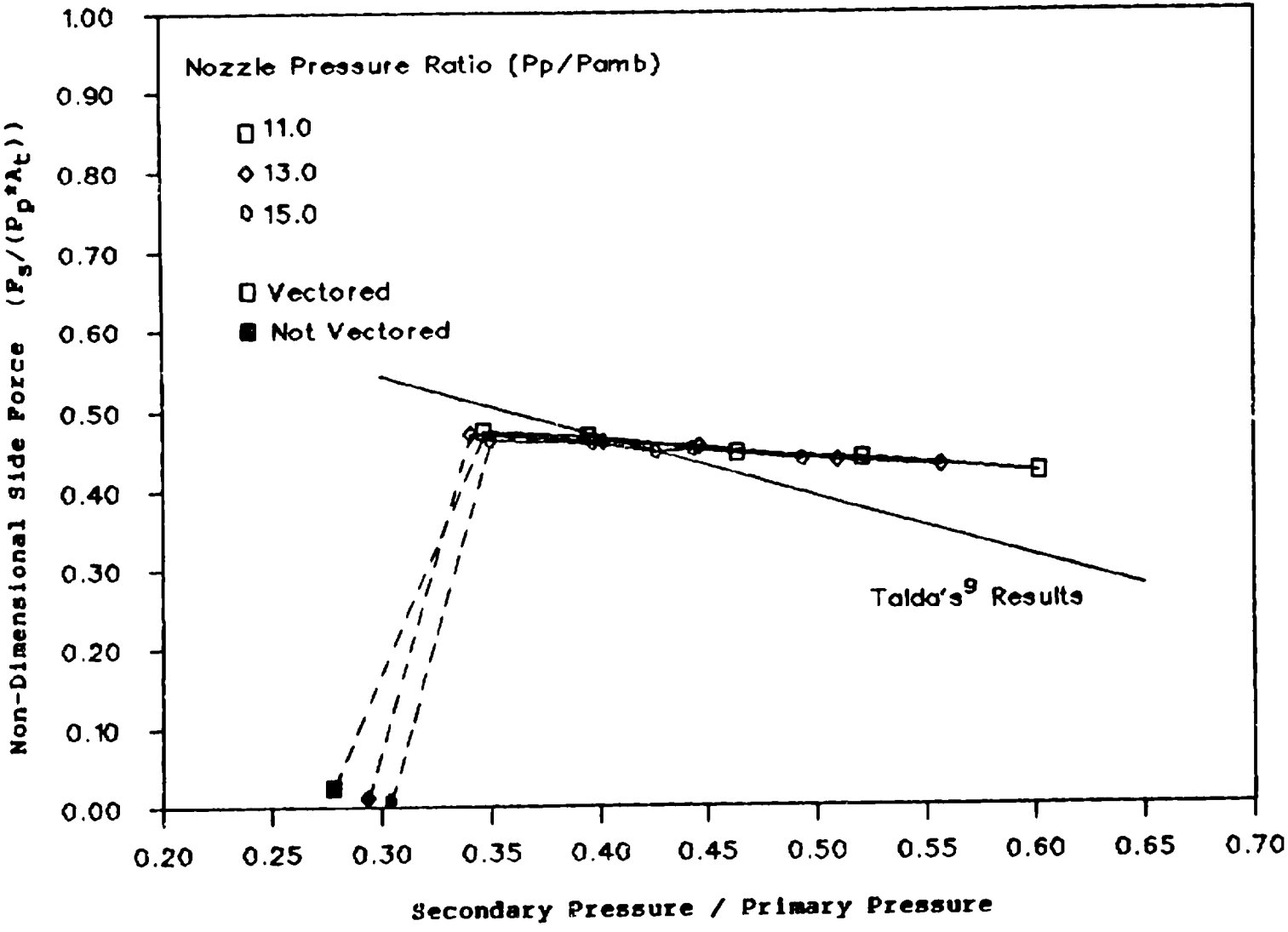

Figure 18. Vectoring Performance, Nozzle 53530(2), Secondary Ports Located at 0.75" from Nozzle Throat

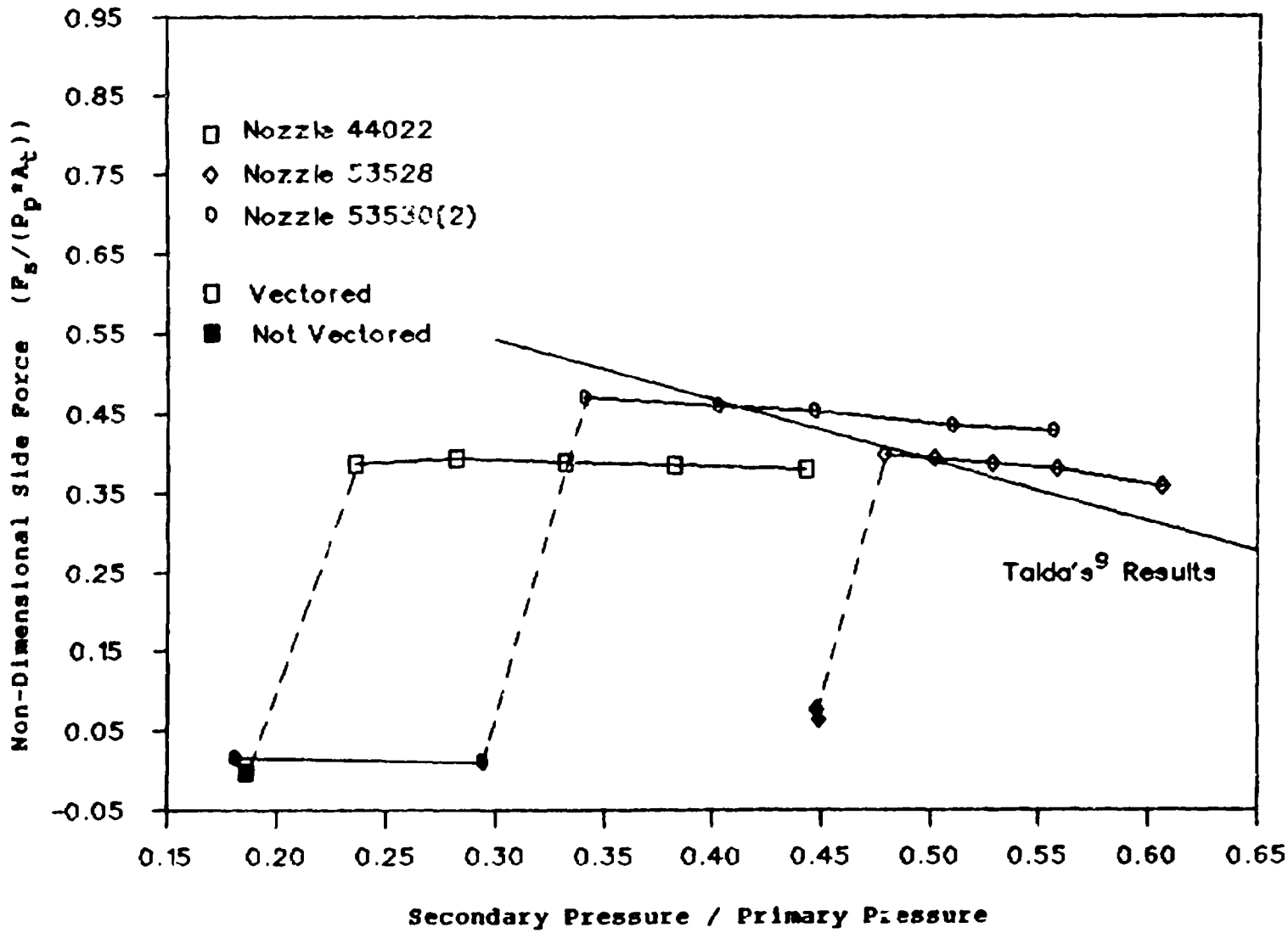

Figure 19. Comparison of Vectoring Performance, Nozzle Pressure Ratio (P_p/P_{amb}) = 13.0

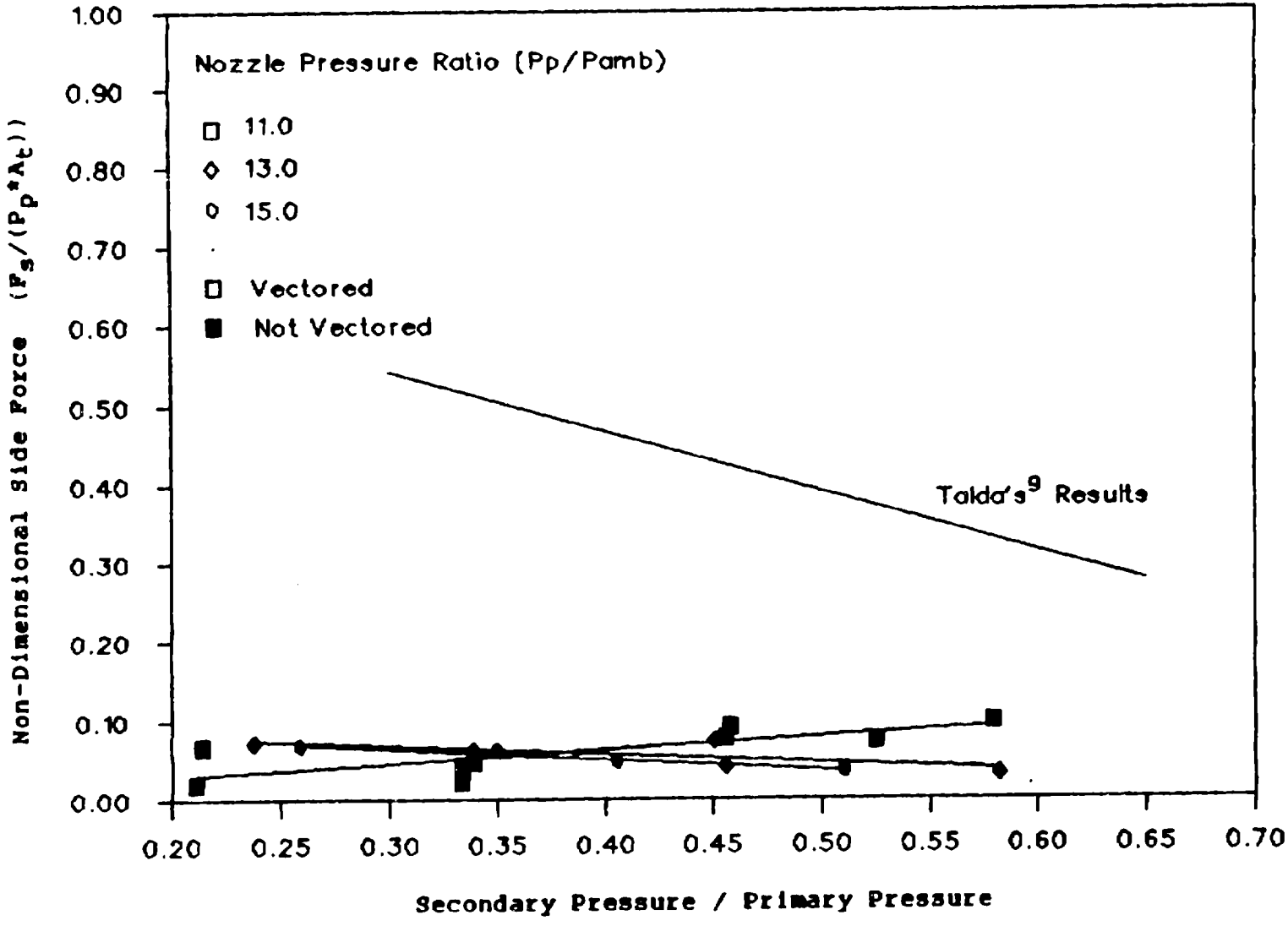

Figure 20. Vectoring Performance, Nozzle 54028, Secondary Ports Located at 1.00" from Nozzle Throat

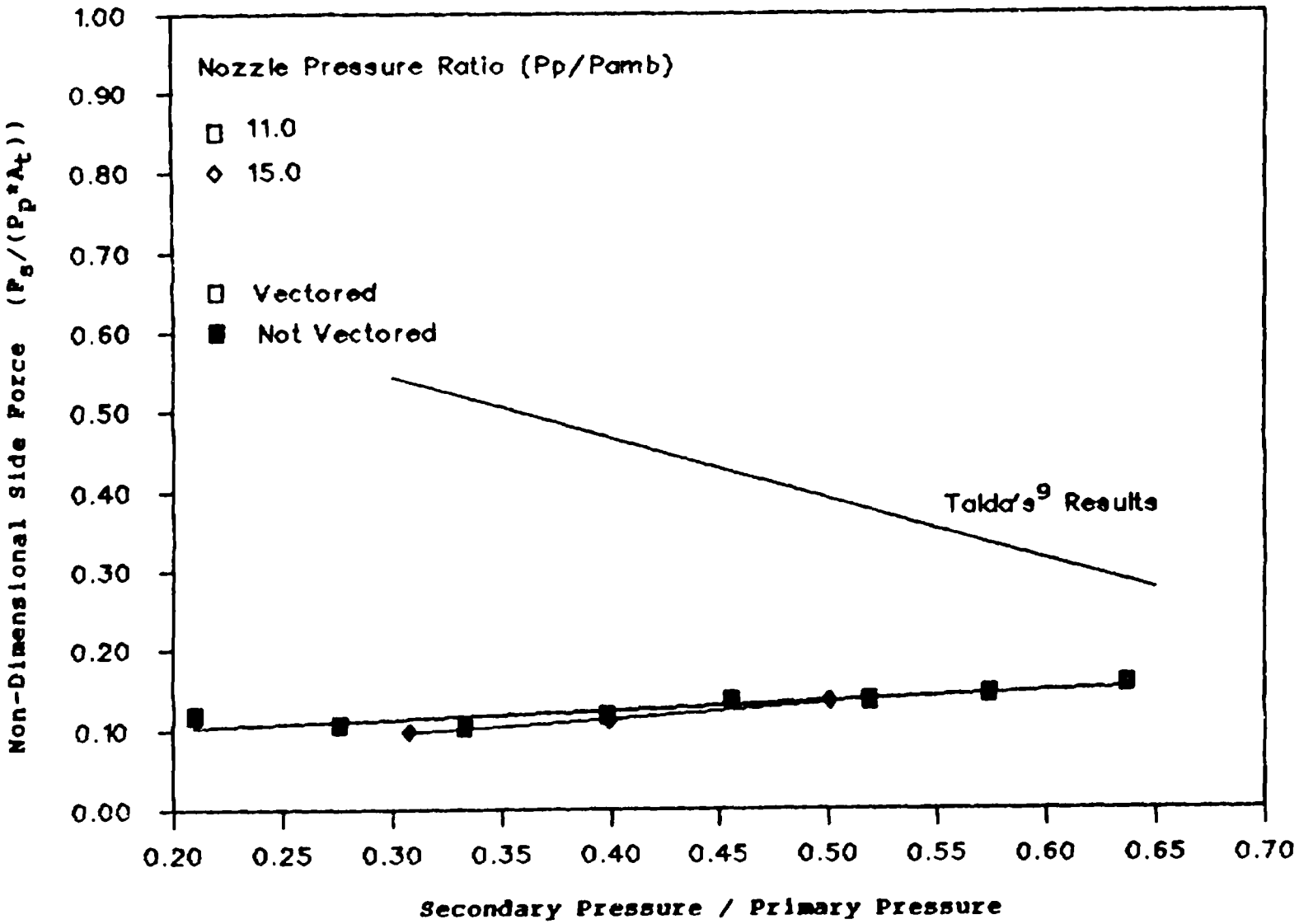

Figure 21. Vectoring Performance, Nozzle 54523, Secondary Ports Located at 1.00" from Nozzle Throat

secondary ports, because this nozzle was unstable over the entire operating range.

Figure 16 shows the vectoring results for nozzle 44022 compared with Talda's[9] results. The solid line in Figures 16 to 21 represent an equation, developed by Talda, to summarize the vectoring results for a 2-D CJTVC nozzle with a secondary injection-to-nozzle throat area ratio (A_{si}/A_t) of 0.20. The results of nozzle 44022 show that the minimum pressure requirements for vectoring (P_{si}/P_p=0.22-0.27) were similar to Talda's results (P_{si}/P_p=0.25-0.30), but the side force was substantially lower and almost constant over the entire operating range. In contrast, the results for nozzle 53528 (Figure 17) show that, while the pressure requirements for vectoring were significantly increased (P_{si}/P_p=0.45-0.50), the side force produced by this nozzle was the same or greater than the results reported by Talda. Finally, the results for nozzle 53530(2) (Figure 18) show that while the minimum pressure requirement (P_{si}/P_p) for vectoring was about 0.34, the side force produced by this nozzle could be greater or less than the results obtained by Talda, depending upon the operating conditions.

The results in Figures 16 to 18 also show that the vectoring performance is independent of the primary pressure, which is similar to the results reported by Talda. Figure 19 shows a comparison of the vectoring results for the nozzles discussed in the previous paragraph. The results in Figure 19 show that small changes in the nozzle geometry can have a

significant impact on the vectoring performance of these nozzles. This figure also indicates that additional testing is required to determine the effect of each design variable on the vectoring performance of 2-D CJTVC nozzles.

The results for nozzles 54028 and 54523 are shown in Figures 20 and 21. Nozzle 54028 (Figure 20) produced little, if any, side force over the entire range of conditions tested. In addition, the characteristic of side force being independent of pressure ratio was not evident for this nozzle. The results for nozzle 54523 (Figure 21) showed that, although this nozzle did not vector completely, there was a slight increase in side force as the secondary pressure was increased.

The measured thrust vector angle (arctangent of the side force divided by the axial force) for nozzles 44022, 53528 and 53530 are shown in Figures 22 to 24. These figures show that while thrust vector angles of 18-22 degrees were obtained for nozzles 44022 and 53528, nozzle 53530(2) produced vector angles of 17-35 degrees. Generally, the vectoring results for these nozzles show that they are less sensitive to changes in the secondary-to-primary pressure ratio (P_{si}/P_p) than the nozzle tested by Talda. Figure 25 shows a comparison of the thrust vector angle for the nozzles discussed above. The results in Figure 25 show that the thrust vector angle is primarily a function of nozzle geometry and that additional testing is required to quantify

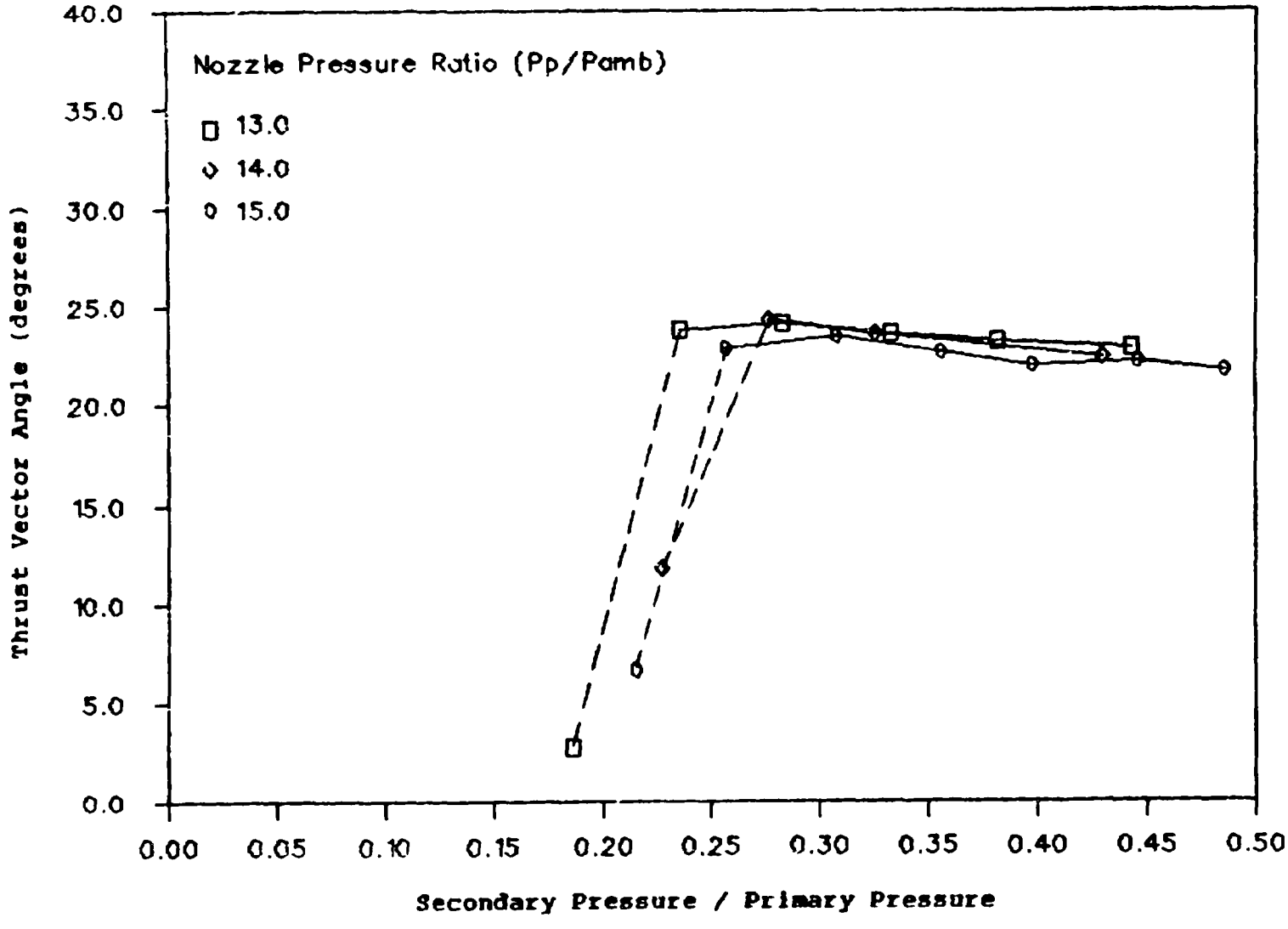

Figure 22. Thrust Vector Angle, Nozzle 44022, Secondary Ports Located at 0.50" from Nozzle Throat

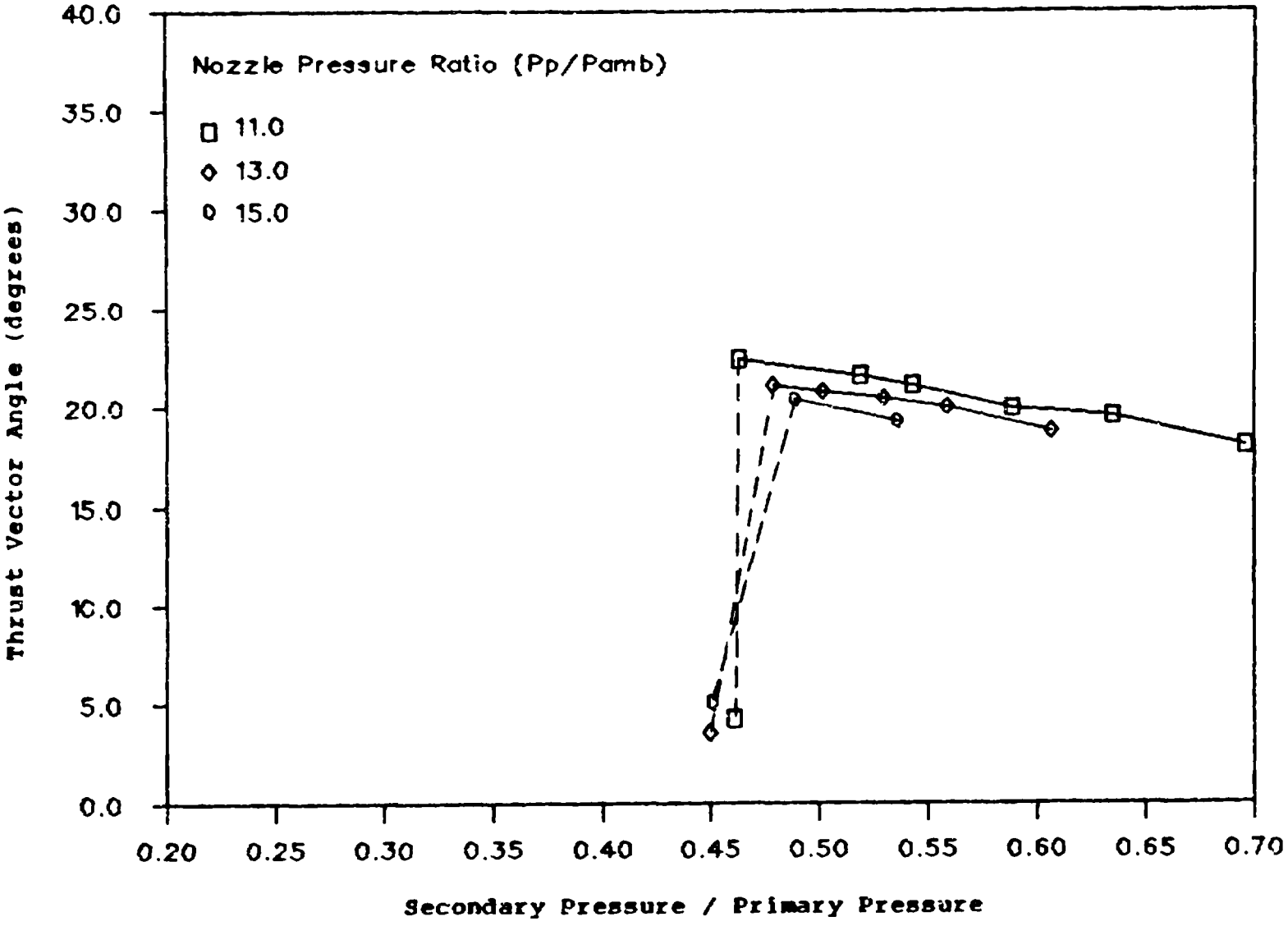

Figure 23. Thrust Vector Angle, Nozzle 53528, Secondary Ports Located at 0.75" from Nozzle Throat

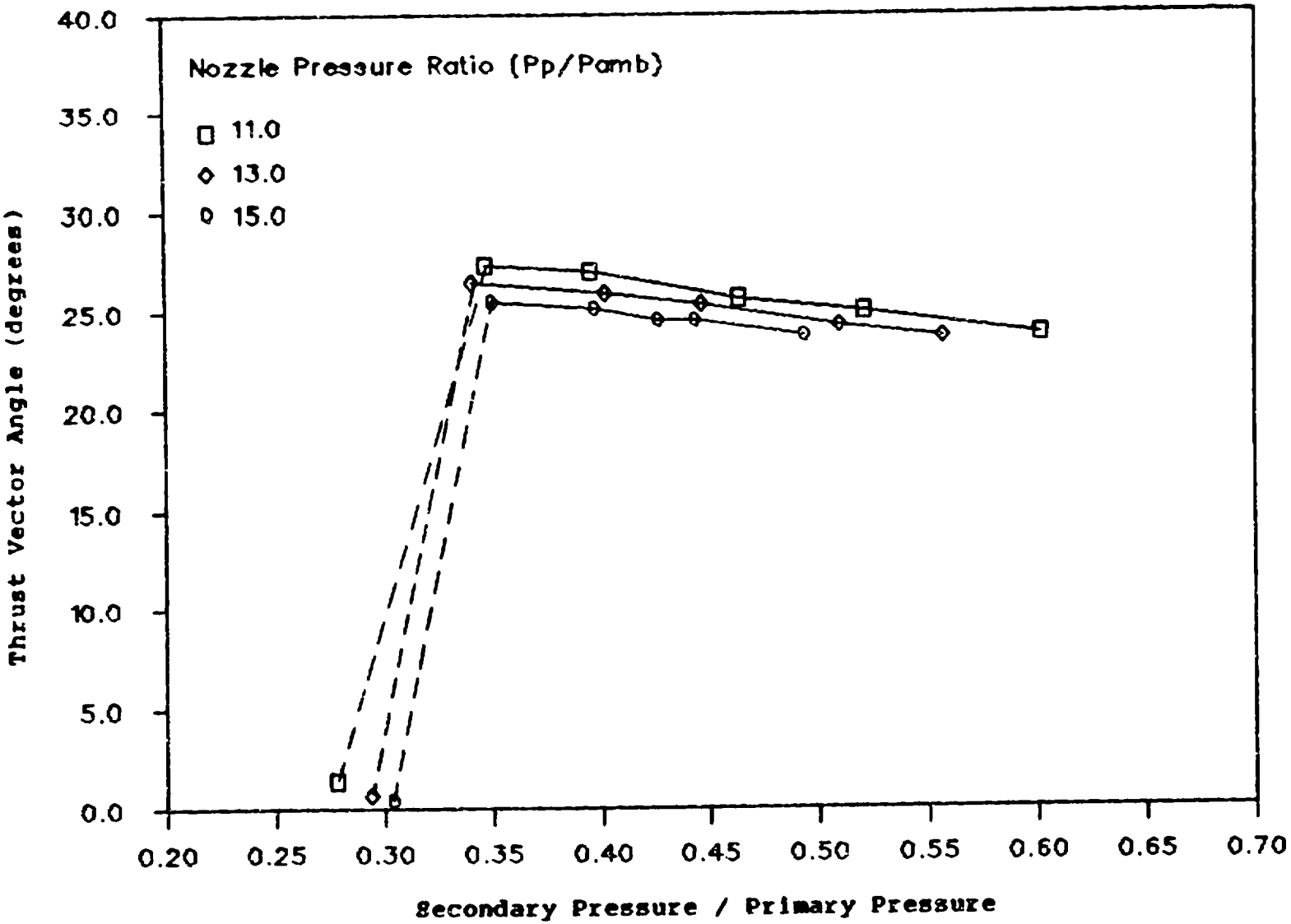

Figure 24. Thrust Vector Angle, Nozzle 53530(2), Secondary Ports Located at 0.75" from Nozzle Throat

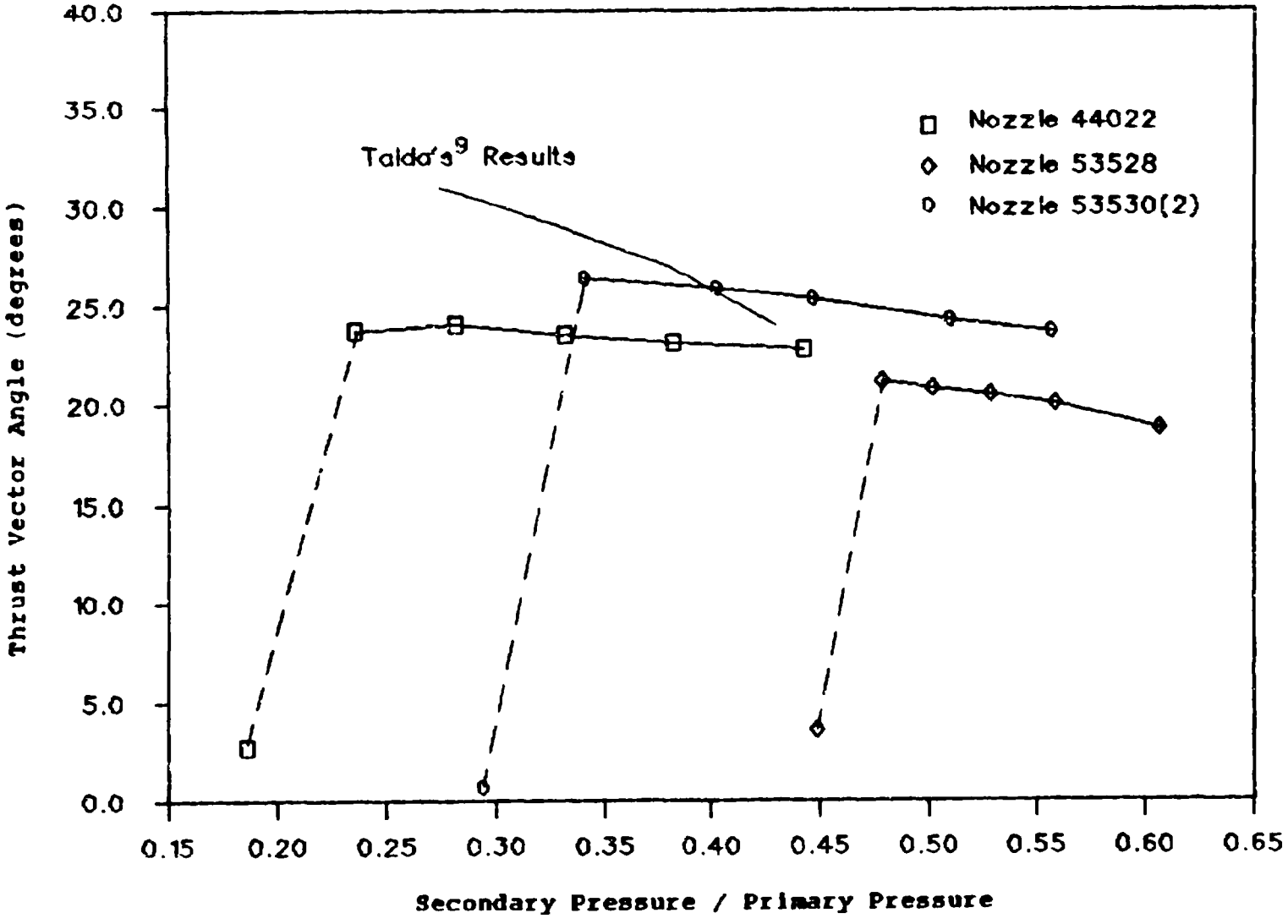

Figure 25. Comparison of Thrust Vector Angle, Nozzle Pressure Ratio (P_p/P_{amb}) = 13.0

these effects.

Effect of Exit Height

Figures 26 and 27 show that small variations in exit height have little effect on the vectoring performance or operability of CJTVC nozzles. The effect of exit height variations were tested on nozzles 53530 and 54028. The results for nozzle 53530 (Figure 26) show that as the exit height is decreased, there is little or no change in side force. However, there is a limit to the amount of exit height variation allowed. For example, when the exit height for nozzle 53530 was reduced from 1.05" to about 0.95", the flow was attached to one side of the nozzle throughout the entire operating range.

The effect of exit height variations on nozzle 54028 are shown in Figure 27. The results in Figure 27 show that this nozzle produced very little side force over the entire operating range, regardless of the exit height.

Effect of Port Location

The secondary port location has a significant effect on the vectoring performance and operability of CJTVC nozzles. These results are similar to those reported by Fitzgerald and Kampe[3]. Both nozzles 53530 and 54523 were tested with two different secondary port locations.

Figure 28 shows the vectoring results for nozzles 53530(2) (secondary ports located at 3/4") and 53530(3) (secondary ports located at 1 1/4") at a NPR of 11.0. The

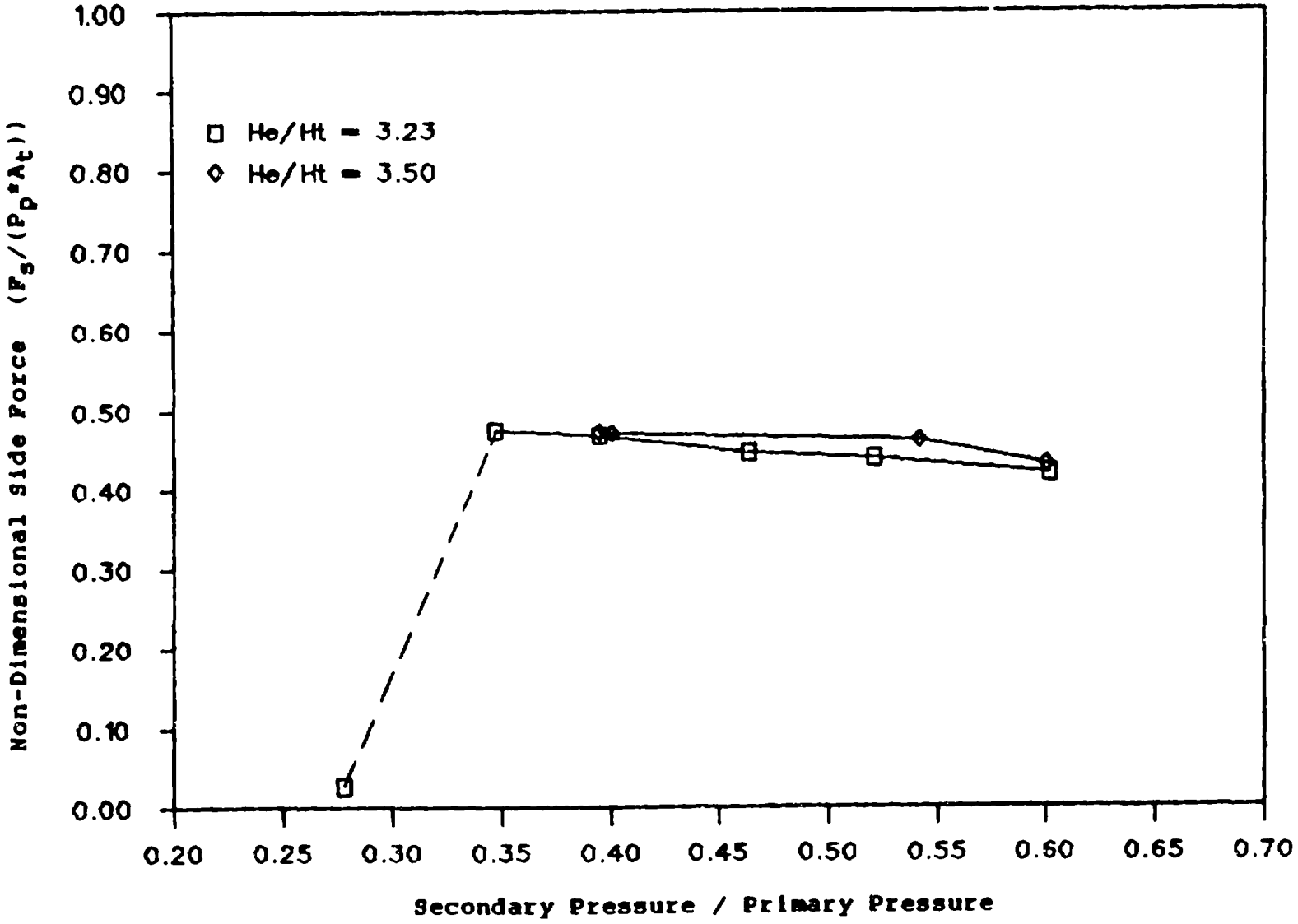

Figure 26. Effect of Exit Height on Vectoring Performance, Nozzle 53530, Nozzle Pressure Ratio (P_p/P_{amb}) = 11.0

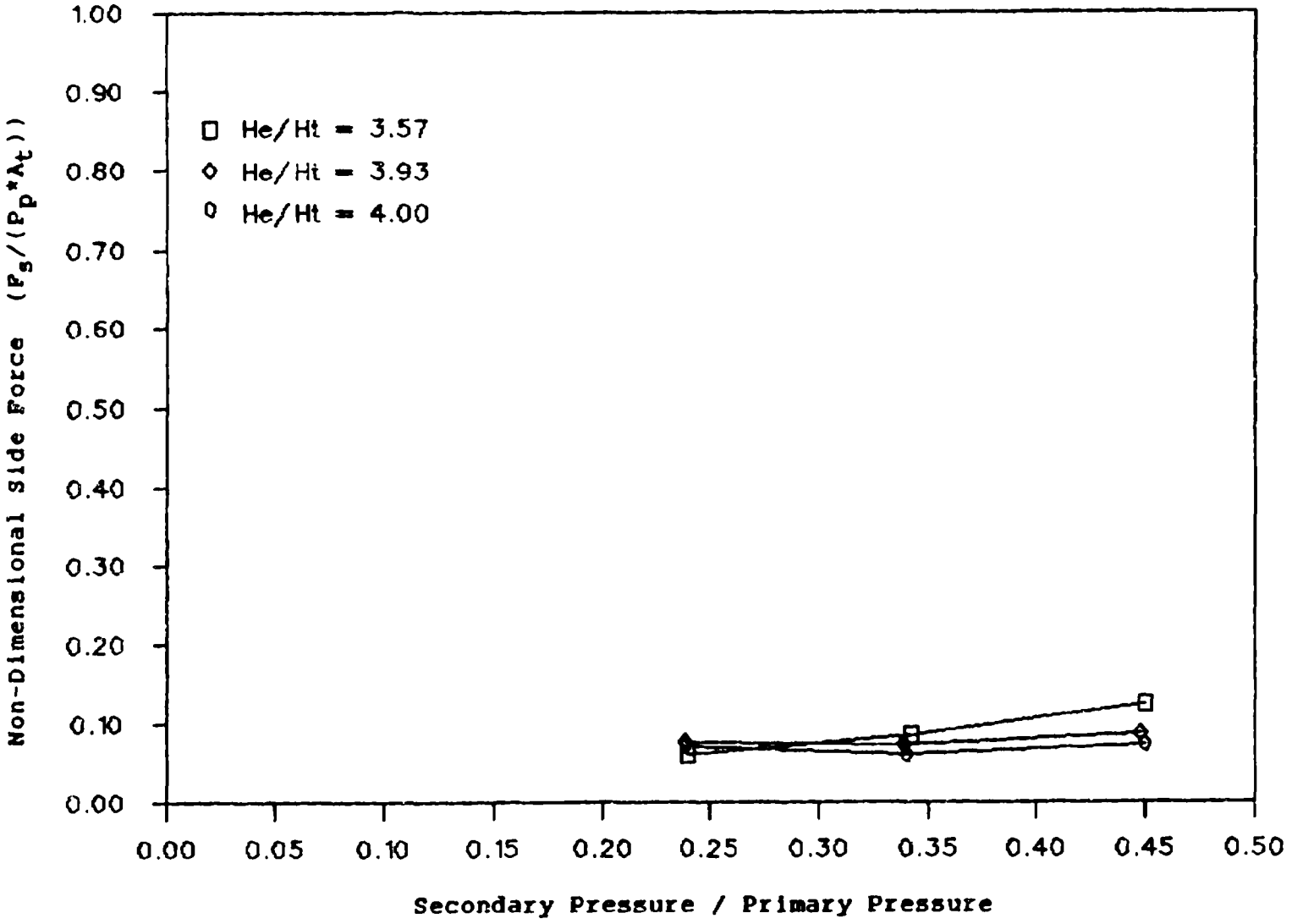

Figure 27. Effect of Exit Height on Vectoring Performance, Nozzle 54028, Nozzle Pressure Ratio (P_p/P_{amb}) = 11.0

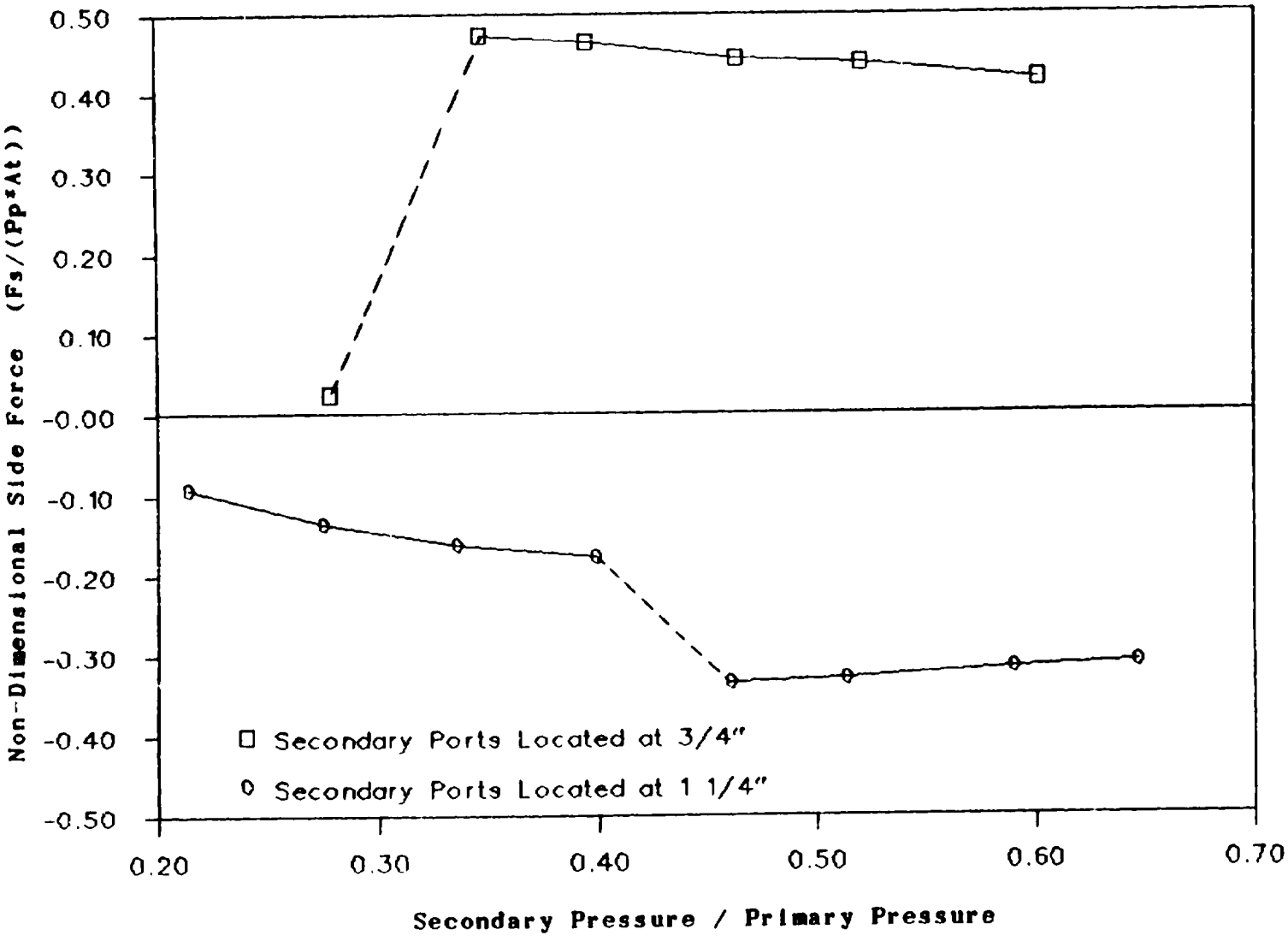

Figure 28. Effect of Port Location on Vectoring Performance, Nozzle 53530, Nozzle Pressure Ratio = 11.0

results in Figure 28 show that when the secondary ports were located at 3/4" the nozzle operated as expected. However, when the ports were located at 1 1/4" the resultant side force was in the opposite direction of what was expected. Figure 29 is a schematic representation of the internal flow field for nozzle 53530(2) (Figure 29(a)) and the results obtained for nozzle 53530(3) are shown in Figure 29(b). Figure 29(b) shows that the secondary stream couples with the separated flow and causes the main jet to reattach to the wall near the secondary port, instead of forcing the jet to the opposite wall. This interaction between the secondary and primary stream is not clear and additional work is required to fully understand these interactions and their benefits, if any, to the vectoring performance of these nozzles.

Results for nozzles 54523 (secondary ports located at 1") and 54523(2) (secondary ports located at 1 1/4") are shown in Figure 30. This figure shows that nozzle 54523 produced very little side force over the entire operating range. However, nozzle 54523(2) produced significantly greater side force but in the opposite direction of what was expected, similar to nozzle 53530(3).

The vectoring results for nozzles 53530(3) and 54523(2) show that there are more operating conditions for 2-D CJTVC nozzles than were previously discussed. Additional testing of these operating modes is required to determine if there are any benefits from this type of operation.

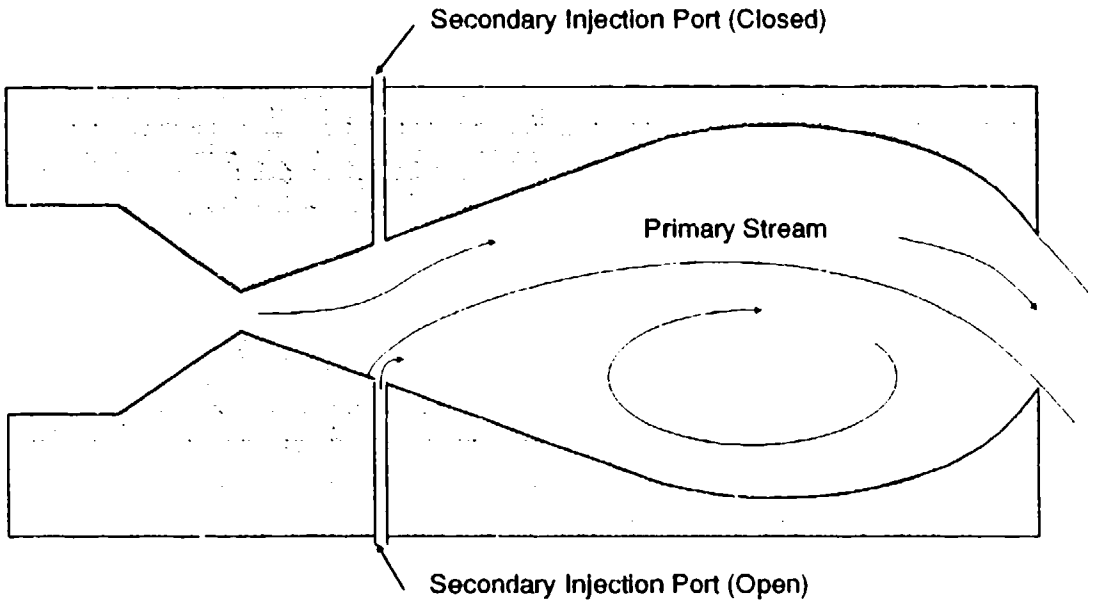

(a) SI Ports Located Upstream of Separation Point

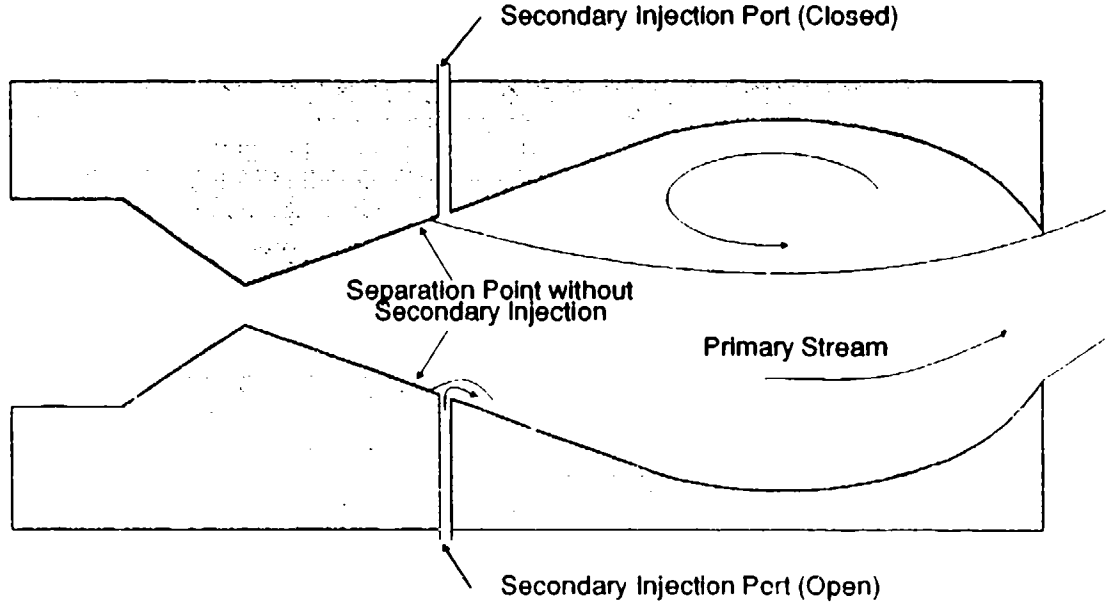

(b) SI Ports Located Downstream of Separation Point

Figure 29 Illustration of CJTVC Vectoring Modes

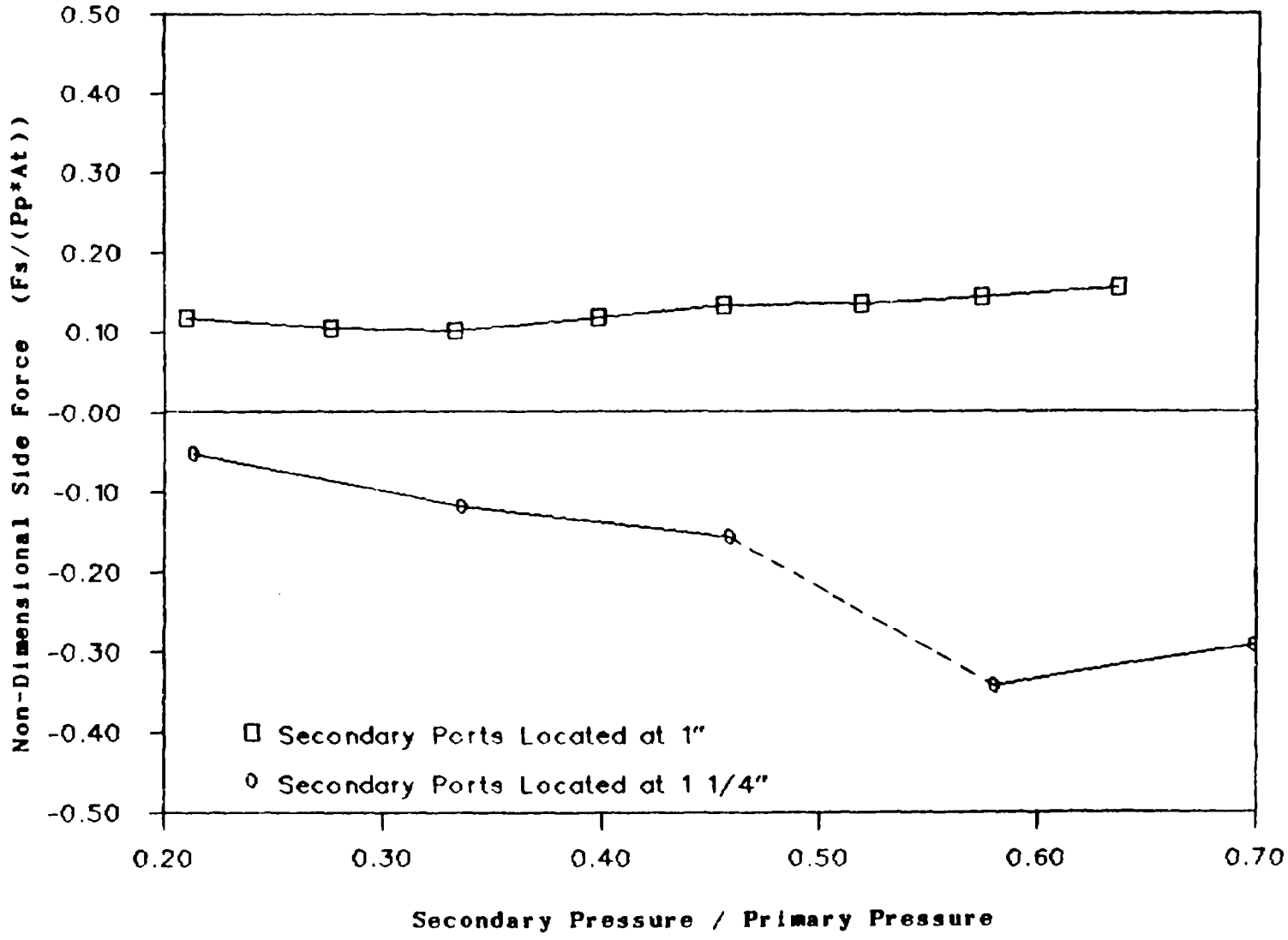

Figure 30. Effect of Port Location on Vectoring Performance, Nozzle 54523, Nozzle Pressure Ratio = 11.0

Design Guidelines for CJTVC Nozzles

The results of the vectoring tests showed that although most of the nozzles were near the range specified by Talda[9] (Figure 31), only three of the nozzles tested vectored using secondary injection. Two of the nozzles (44022 and 53528) that vectored were slightly outside this range, while the other nozzle (53530) was within the range (Figure 31). Figure 31 also shows that nozzle 44020, which has the same characteristics as the nozzle that vectored during Talda's tests, did not vector. In addition, Talda did not provide any information on the placement of secondary ports. These results show that the critical design parameter suggested by Talda, nozzle length divided by exit height, is inadequate for designing 2-D CJTVC nozzles and new design guidelines for these nozzles needs to be established.

A review of the design variables for all the nozzles in this study and in Talda's study revealed new design guidelines for 2-D CJTVC nozzles (Figure 32). Figure 32 shows that the design parameters include: secondary port location, nozzle length, exit height and throat height. Notice that these new guidelines do not include the effect of divergence or exit angle. The divergence and exit angle were held constant for all the nozzles tested and additional testing would be required to define their impact on the nozzle design.

The results shown in Figure 32 include the nozzles in

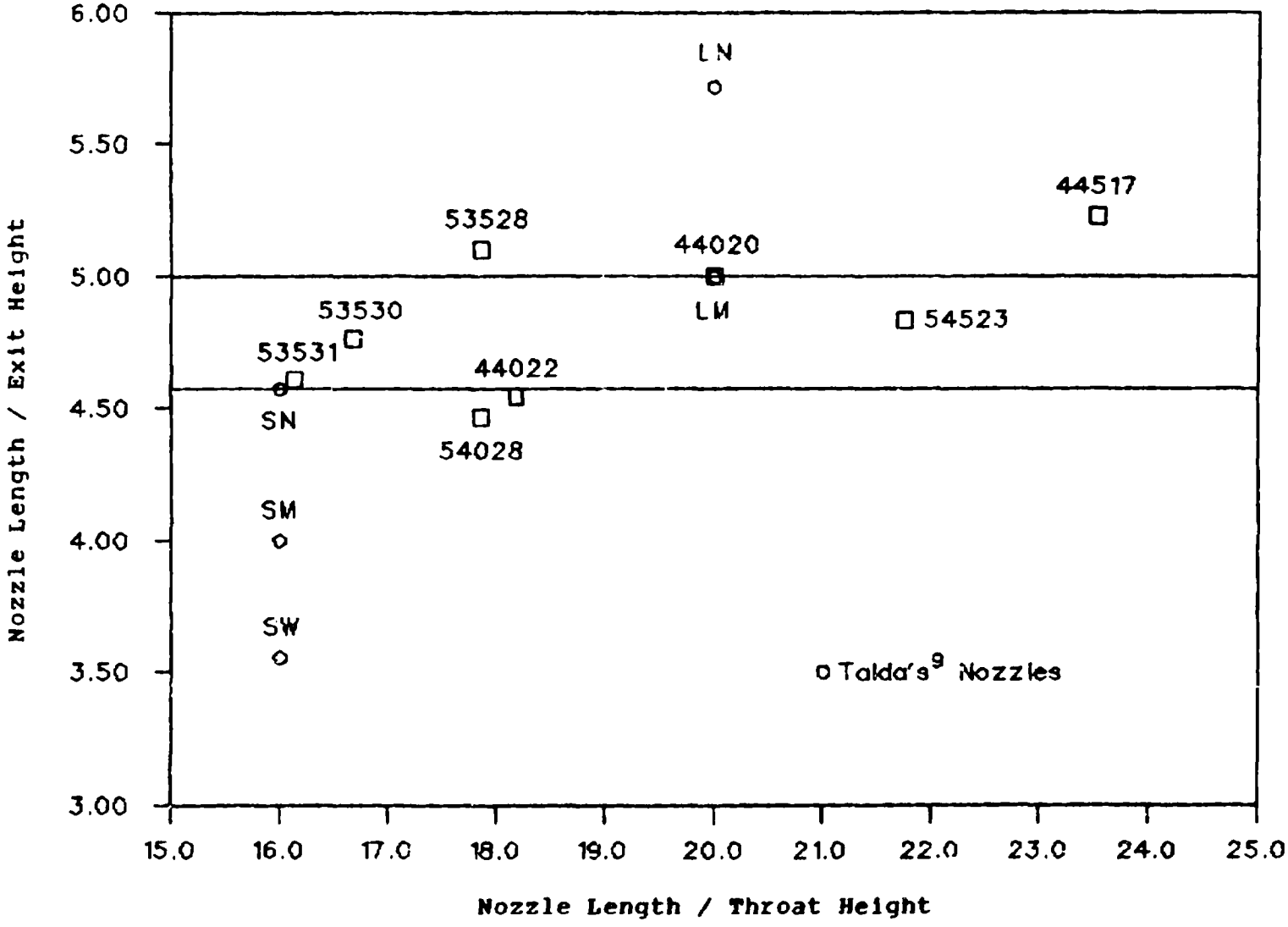

Figure 31. Design Guidelines for 2-D CJTVC Nozzles (Talda[9])

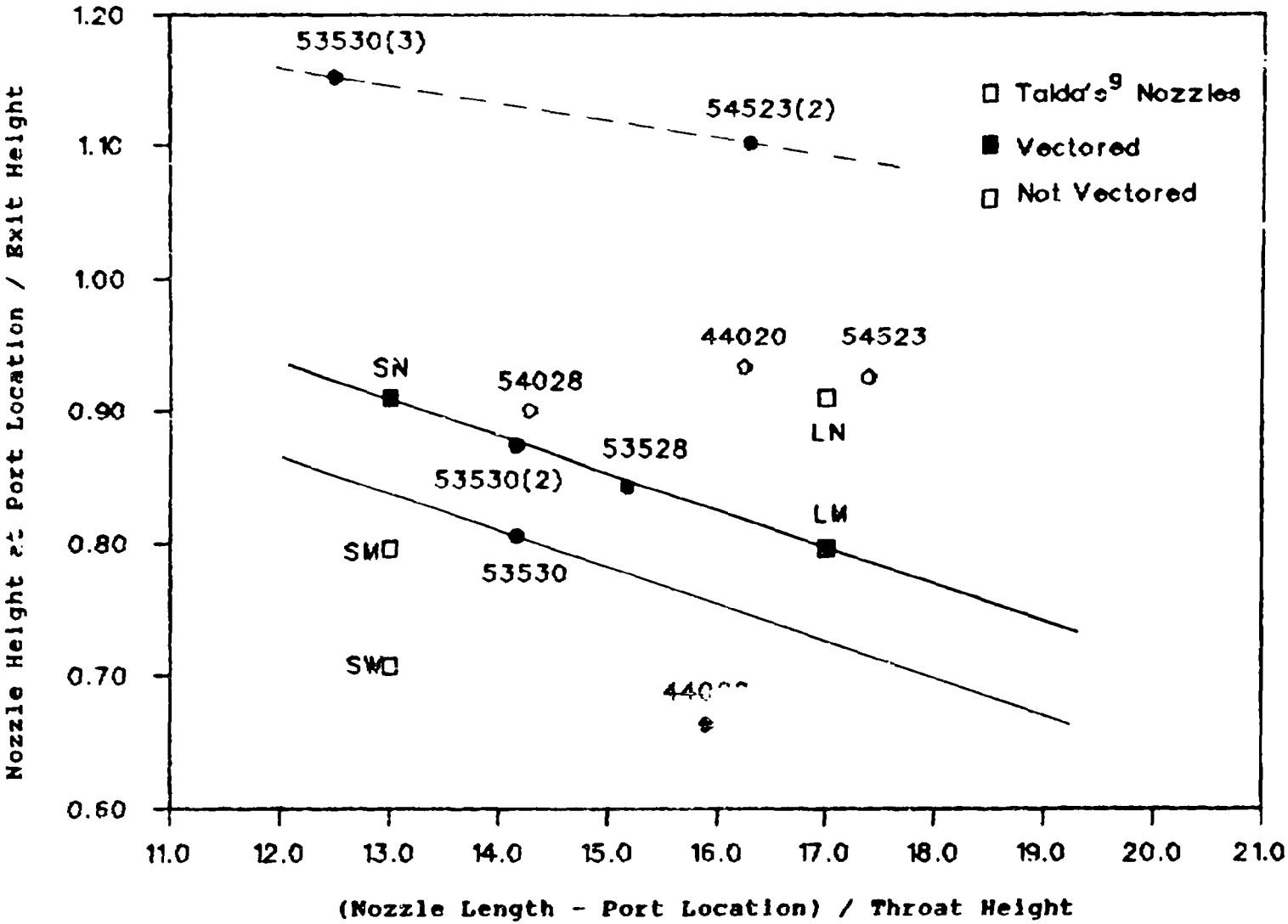

Figure 32. Revised Design Guidelines for 2-D CJTVC Nozzles

the present study, as well as those tested by Talda. The darkened symbols in Figure 32 represent the nozzles that could be vectored using secondary injection and the solid lines represent a "best guess" of the allowable range for the two non-dimensionalized design parameters. Although most of the nozzles that vectored were within this range, the vectoring performance of all these nozzles were slightly different. The reasons for these differences are not evident from the available data and additional testing is required in order to provide a satisfactory answer.

Figure 32 also shows that, although nozzle 44022 vectored, it does not lie in the region defined by the solid lines. Test results for this nozzle showed that during some test conditions, without secondary flow injection, the flow vectored rapidly from one nozzle wall to the other. These results suggest that this nozzle is on the verge of being unstable and even a small change to the internal flow field of the nozzle could cause vectoring.

The dashed line in Figure 32 is shown to represent an estimate for the design parameters for the nozzles that vectored in the direction opposite of what was expected. Again, the benefits, if any, of this type of operation for these nozzles need additional testing.

Effect of Secondary Ports on Axial Performance

One of the most important performance parameters for any type of nozzle is the axial thrust efficiency. The

results for most of the nozzles tested are shown in Figures 9 and 10. However, these results are for nozzles without secondary ports. Therefore, it is important to determine what the effect of adding secondary ports is on nozzle axial efficiency. The results for several nozzles with and without secondary ports are shown in Figures 33 to 35.

The results for nozzle 54523 are shown in Figure 33. These results show that there is little, if any, penalty in axial thrust for adding secondary ports. However, these results are for a nozzle where the secondary ports are located downstream of the separation point.

The results for nozzle 53528 (Figure 34) show that at low NPRs the addition of secondary ports has no effect on the nozzle axial efficiency. However, as the NPR is increased the axial efficiency drops sharply and then begins to rise again. The reason for this is not clear, but it may be that at the low NPRs the flow is separating before it reaches the secondary ports. When the NPR is increased the separation point moves downstream until it reaches the secondary port and the interaction between the secondary port and the separation point results in a 5-8% decrease in axial efficiency.

Results for nozzle 44022 are shown in Figure 35. These results show that adding secondary ports to the nozzle had very little impact on the axial efficiency. This contradicts the explanation of the results for nozzle 53528. The results for nozzle 53528 suggested that there was an

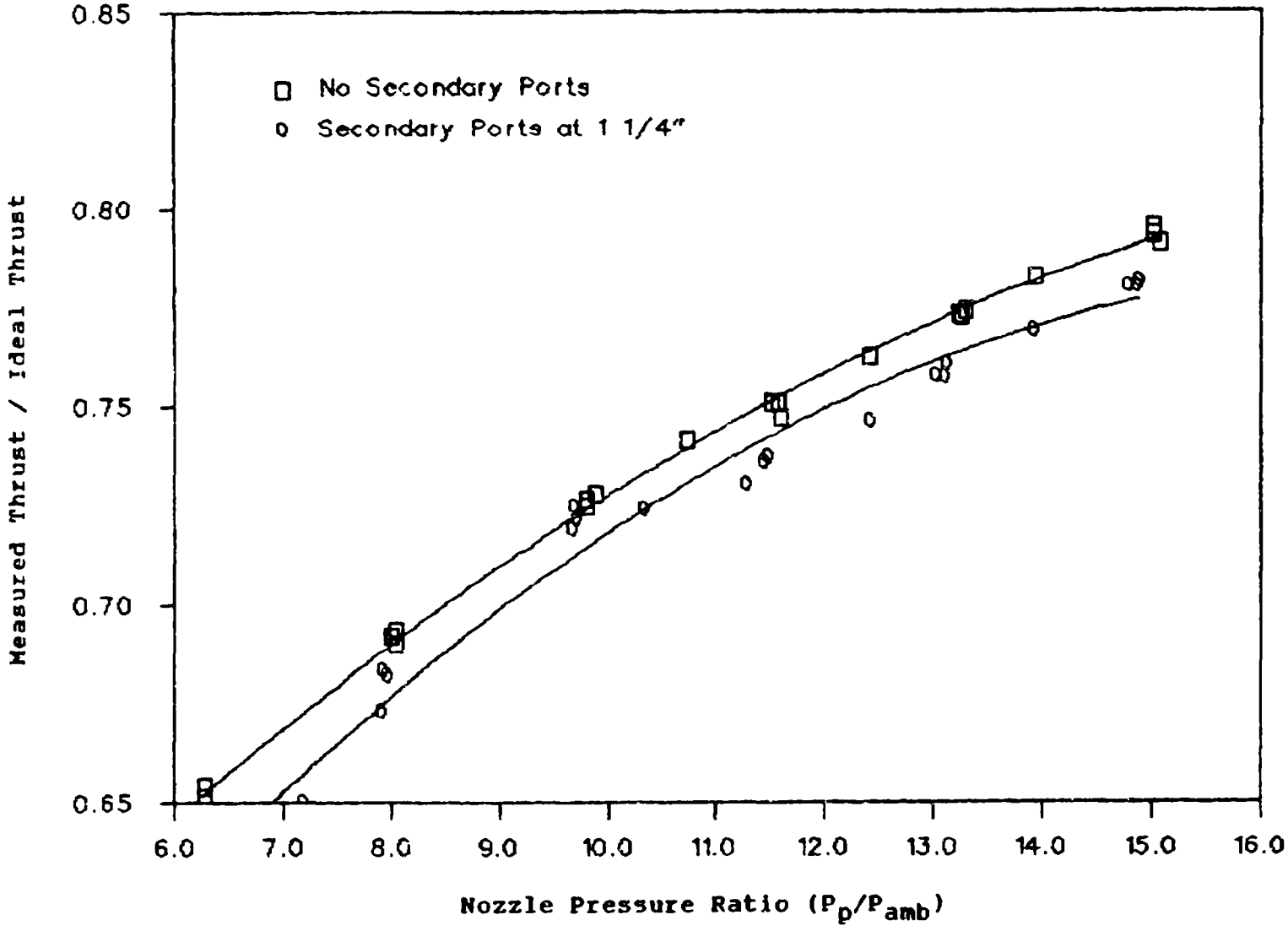

Figure 33. Effect of Secondary Ports on Axial Efficiency, Nozzle 54523

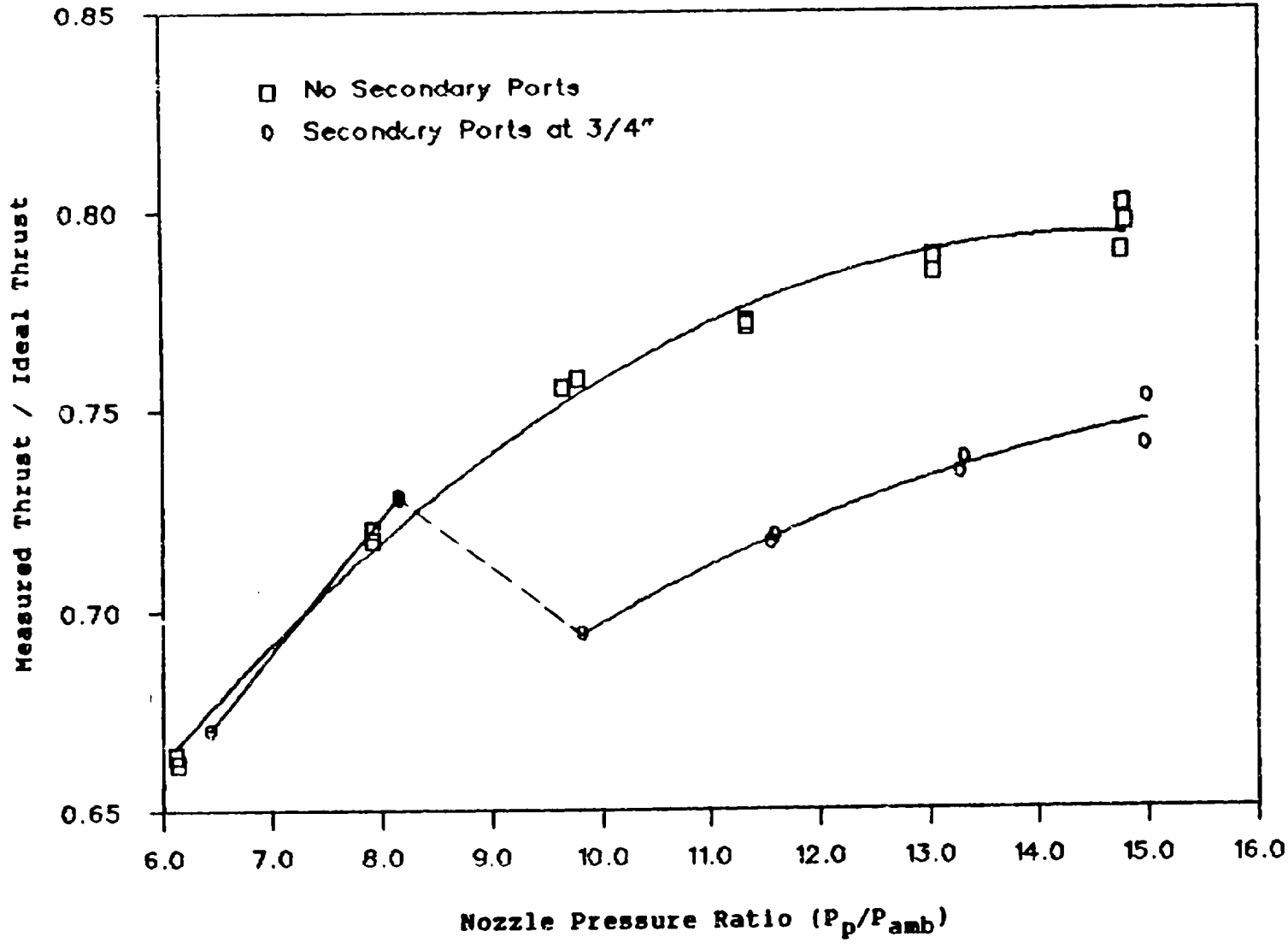

Figure 34. Effect of Secondary Ports on Axial Efficiency, Nozzle 53528

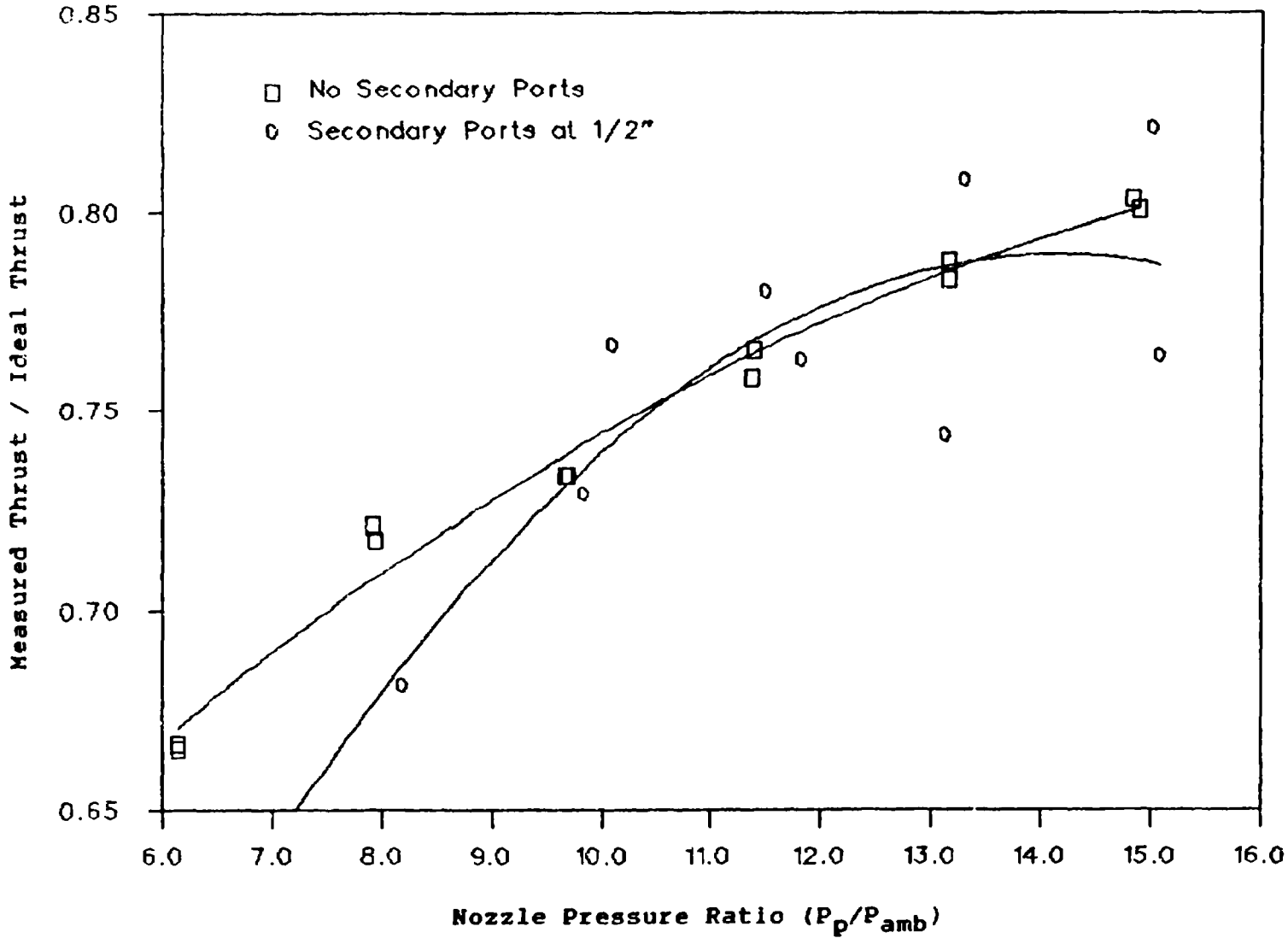

Figure 35. Effect of Secondary Ports on Axial Efficiency, Nozzle 44022

interaction between the separation point and secondary port at a NPR of about 9.0. However, no such interaction was evident for nozzle 44022 even though the separation point, without secondary ports, was at about 3/4" and the secondary ports were located at 1/2". These results indicate that additional tests need to be conducted to establish the effect of secondary ports on axial efficiency.

V. Conclusions

Based on the tests results presented in this study, the following conclusions are made:

1. Two-dimensional CJTVC nozzles can provide axial thrust ratios (measured thrust divided by ideal thrust) of about 0.80, depending on NPR and exit area ratio (exit area divided by throat area).

2. The exit area ratio has a significant impact on the maximum achievable axial efficiency. The maximum efficiency increases as the exit area ratio increases, however this also requires a higher NPR.

3. Thompson's[10] analytical method can be used to predict the point of flow separation in two-dimensional CJTVC nozzles, provided the correct pressure ratio (P_p/P_{recirc}) is used.

4. Small changes in exit height (less than about 8%) have little effect on the nozzle performance or vectoring ability.

5. The location of secondary injection ports have a significant effect on the vectoring ability of CJTVC nozzles. Secondary ports located downstream of the separation point tend to pull the main jet toward the port, rather than force it to the opposite wall.

6. The design of two-dimensional CJTVC nozzles, that can be vectored using secondary injection, depend on

appropriate choices for nozzle length, exit area ratio, throat height and secondary port location.

7. Thrust vector angles of 25 degrees are achievable with two-dimensional CJTVC nozzles.

VI. Recommendations

Based on the results of this study, the following recommendations are made for further studies of two-dimensional CJTVC nozzles:

1. Fabricate additional two-dimensional CJTVC nozzles to verify the design guidelines established in this report.

2. Incorporate Design of Experiments or Taguchi methods into future studies in order to systematically evaluate the effect of design variables on axial and vectoring performance.

3. Conduct additional studies on 2-D CJTVC nozzles with the secondary ports located downstream of the separation point. The benefits, if any, of this alternate vectoring are unclear. Therefore, additional testing is required to answer this question.

4. Study the effects of changing the divergence and exit angles. Increasing the divergence angle may allow the nozzle length to be reduced.

5. Modify the test stand to allow for the use of the schlieren system at the same time as the side force is being measured.

Appendix A: Uncertainty Analysis

Uncertainty Analysis

An important part of any experimental study is determining the error or uncertainty associated with the data measurements. Measurement uncertainties can result from many sources, such as: the data acquisition system, the calibration process and the equipment used during the calibration process. In this study, the uncertainty analysis was limited to estimating the uncertainty between the calibration data and a linear curve fit calculated for this data.

Prior to conducting any tests, the pressure transducers and the force balance (axial and side force) were calibrated over a wide range of pressures and forces, respectively. The range of pressures and forces were selected so that at least one calibration point exceeded the maximum anticipated pressure or force for any test condition.

The calibration results for each pressure transducer and the force balance (axial and side force) were plotted and a linear "least squares" polynomial was calculated for each plot. A review of these results showed that there was good agreement between the calibration data and the curve fits. In general, the calibration data was within about 2% of the linear curve fit. Table II summarizes the "worst case" results for each transducer and the force balance.

Table II Estimation of the Maximum Uncertainties of the Calibration Data Relative to the Linear "Least Squares" Curve Fit

Transducer	Maximum Uncertainty (%)
Static Press. #1	0.8
Static Press. #2	0.7
Static Press. #3	1.4
Static Press. #4	0.3
Static Press. #5	0.2
Static Press. #6	0.4
Static Press. #7	0.7
Static Press. #8	0.4
Static Press. #9	0.3
Static Press. #10	0.3
Static Press. #11	0.3
Static Press. #12	0.1
Primary Press.	0.7
Secondary Press.	2.5
Axial Force	1.8
Side Force	2.3*

* This rose to about 11% as the load was reduced below 2.5 lb_f

Appendix B: Ideal Thrust Calculations

Ideal Thrust Calculations

The equation for calculating gross thrust, provided by Sutton[8], was:

$$F_g = \dot{m}V_e + (P_e - P_{amb})A_e \qquad (1)$$

The ideal thrust was calculated by assuming one-dimensional, isentropic expansion through a converging-diverging nozzle. Assuming the flow was fully-expanded (exit pressure equal to ambient pressure) Equation (1) then becomes:

$$F_i = \dot{m}V_e = (\rho_t a_t A_t M_e a_e)/g_c \qquad (2)$$

where

$$\rho_t = (P_p/R_1 T_p)(2/(k+1))^{(1/(k-1))}$$

$$a_t = ((2kR_2T_p)/(k+1))^{1/2}$$

$$A_t = H_t * W_t$$

$$M_e = ((2/k-1)((P_p/P_{amb})^{((k-1)/k)}-1))^{1/2}$$

$$a_e = (kR_2T_p(P_{amb}/P_p)^{((k-1)/k)})^{1/2}$$

$$g_c = 32.174 \ lb_m\text{-}ft/lb_f\text{-}sec^2$$

$$k = 1.4$$

$$R_1 = 0.3704 \ psia\text{-}ft^3/lb_m\text{-}^oR$$

$$R_2 = 1716.0 \ ft^2/sec^2\text{-}^oR$$

Appendix C: Calculation of Flow Separation Point

Calculation of Flow Separation Point

The flow separation point was calculated by using an analytical method derived by Thompson[10]. This method was developed by the equating momentum forces for a compressible, turbulent boundary layer to the applied back pressure. The results give an equation for the Mach number at separation, as a function of pressure ratio:

$$M_s^2 = \frac{2}{k-1}\left[\left[\left(\frac{kn}{(n+2)} + 1\right)\left(\frac{P_p}{P_{amb}}\right)\right]^{(k-1)/k} - 1\right] \quad (3)$$

where

k = Specific Heat Ratio (1.4)

n = Velocity Profile Power Law Index (7.0)

Substituting in the values for k and n, reduces Equation (3) to:

$$M_s = (6.17(P_p/P_{recirc})^{0.286} - 5)^{1/2} \quad (4)$$

The area ratio at separation can then be calculated by using the following isentropic area relation:

$$\frac{A}{A_t} = \frac{1}{M_s}\left[\frac{1+((k-1)/2))M_s^2}{(k+1)/2}\right]^{((k+1)/2(k-1)} \quad (5)$$

where

k = Specific Heat Ratio (1.40)

The axial location of the flow separation point is then found by using the following equation:

$$X_s = (1/2\tan(\delta))(H_t(A/A_t)) - H_t) \quad (6)$$

Appendix D: Measurements of the Flow Separation Point

Measurements of the Flow Separation Point

There are several methods that can be used to determine the flow separation point in nozzles. Two different methods, which use the nozzle static pressure distribution, were tried in this study. The first method consisted of plotting the nozzle static pressure, as a function of axial distance from the nozzle throat, for each test condition (Figure 36). This figure shows that the nozzle static pressure first decreases, as the axial distance is increased, and then rises rapidly at some point in the nozzle. Flow separation is assumed to occur at the point where the nozzle static pressure rises rapidly.

The second method, which was also used by Scheller and Bierlein[7] and Friddell and Franke[4], consisted of plotting the nozzle static pressure, for a given pressure tap location, as a function of NPR (Figure 37). The flow separation point was determined by locating the NPR at which the static pressure becomes nonlinear, for any pressure tap. The nonlinearity in the static pressure is caused by the separation point passing the tap location. For example: Figure 37 shows that the static pressure measured at 3/4" becomes nonlinear as the NPR is reduced below 8.0. This shows that when the NPR is below 8.0 the flow separates prior to reaching the pressure tap located 3/4". This method was also used to estimate the maximum axial position of the flow separation. For example: Figure 37 shows that at a NPR of 6.0, the flow has separated prior to reaching the tap located at 3/4" and at the higher NPRs, the flow always separates prior to reaching the tap located at 1".

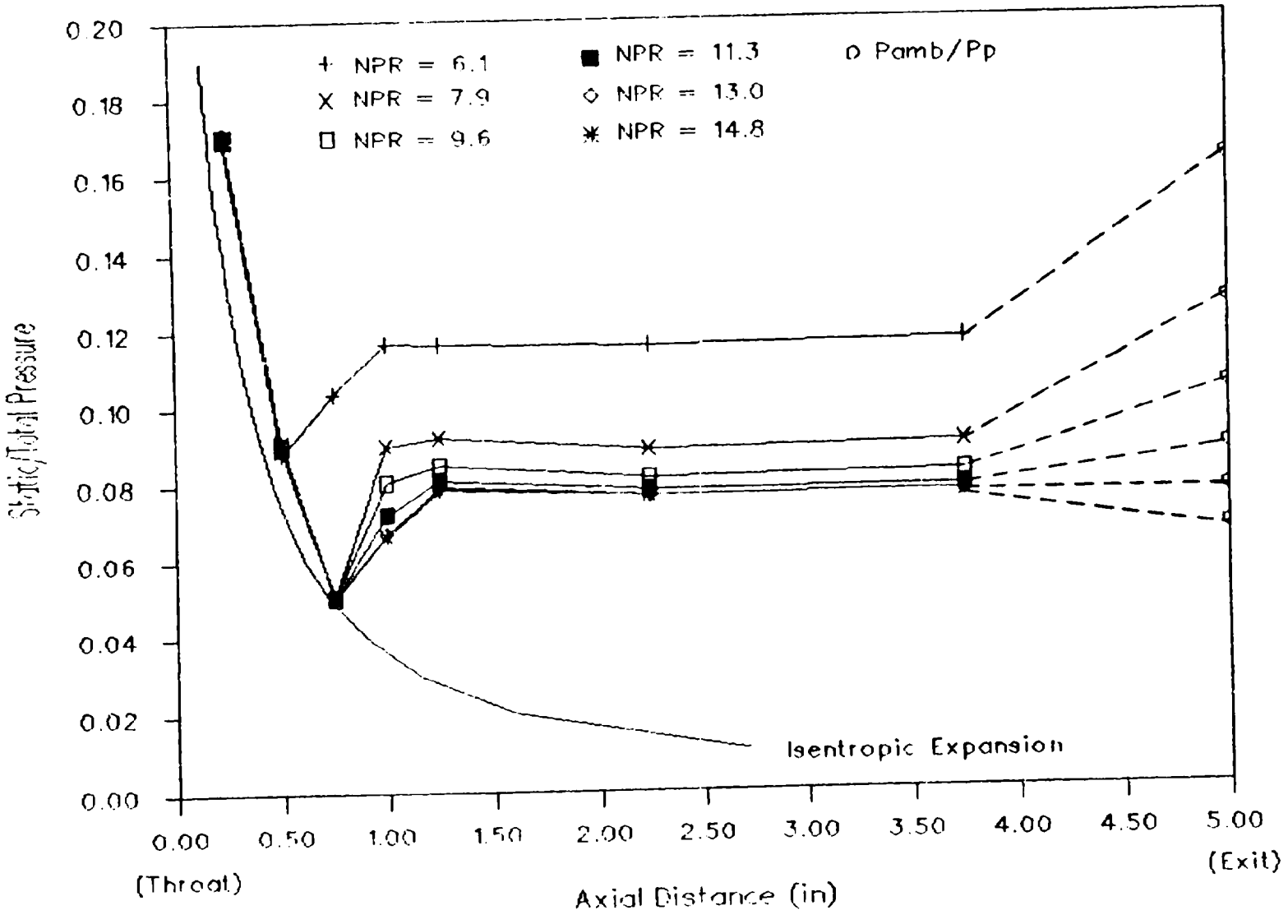

Figure 36 Static Pressure Distribution, Nozzle 53528, No Secondary Ports

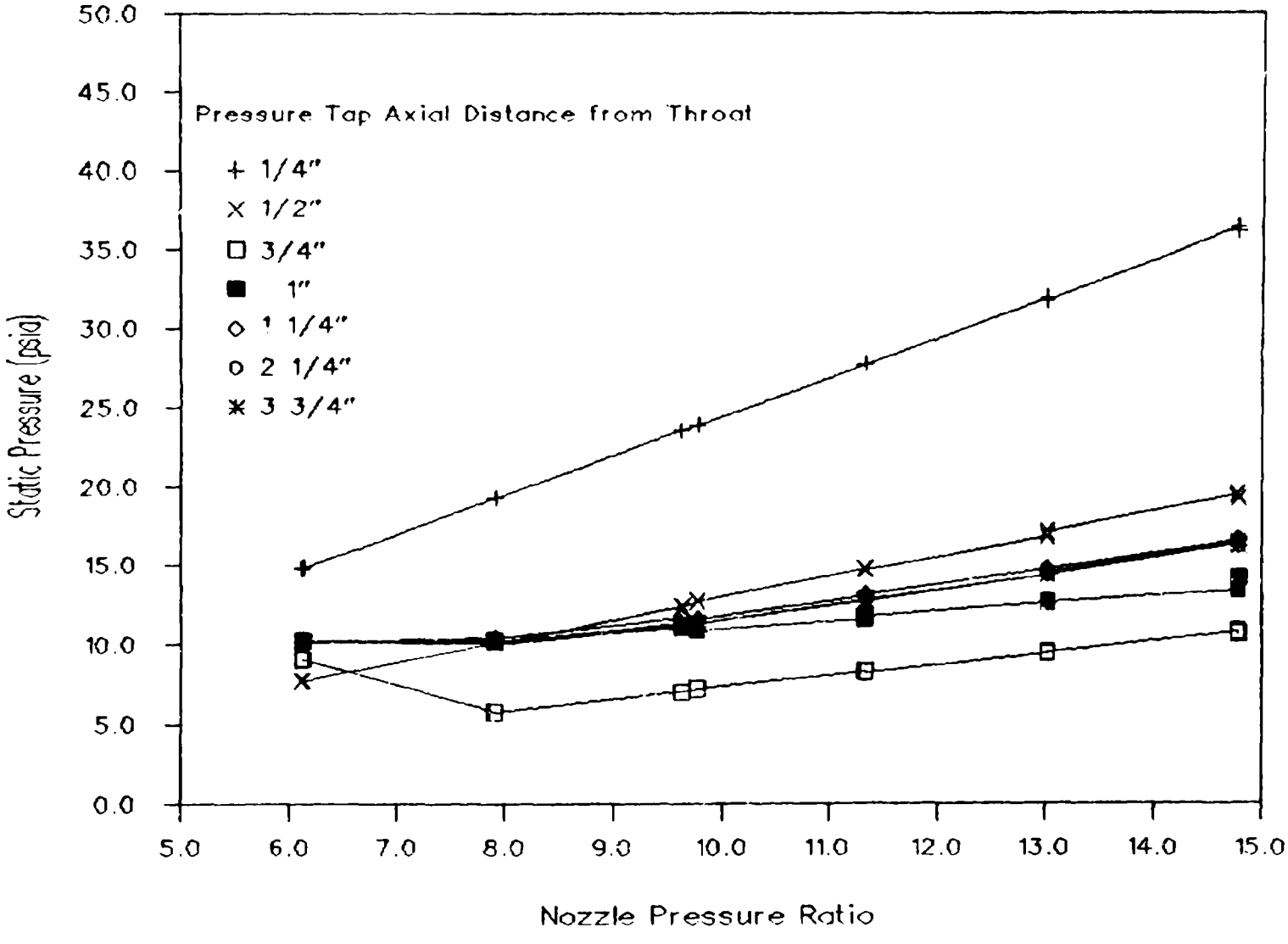

Figure 37 Nozzle Static Pressure, Nozzle 53528, No Secondary Ports

The results of the two previous methods showed that the pressure taps were spaced too far apart to accurately determine the flow separation point. In order to overcome these difficulties, a new method for estimating the separation point, which is a combination of the two previous methods, was developed.

The procedure for this method is as follows: First, Figure 37 was used to accurately locate the separation point in the nozzle (3/4" at a NPR of 7.93). This result was then used to define the pressure gradient, point A to point B, downstream of the separation point (Figure 38). The pressure gradient was assumed to be independent of the NPR and was applied to the nozzle pressure distribution for different NPRs (point C to point D in Figure 38). The flow separation point was then defined as the point at which the pressure gradient intersects the isentropic expansion line (point D, Figure 38).

One of the key assumptions in this method was that the pressure gradient downstream of the separation point is independent of NPR. Figure 39 shows the pressure gradient downstream of the separation point for all the nozzles, except 44517 and 53530. Notice that the pressure gradient is independent of both the NPR and nozzle design, which supports the assumption stated previously.

The procedure outlined above was applied to the results for all the nozzles, except nozzles 44517 and 53530. A comparison between these measured results and those obtained by using Thompson's[10] analytical method are shown in Figures 13 and 40 to 44.

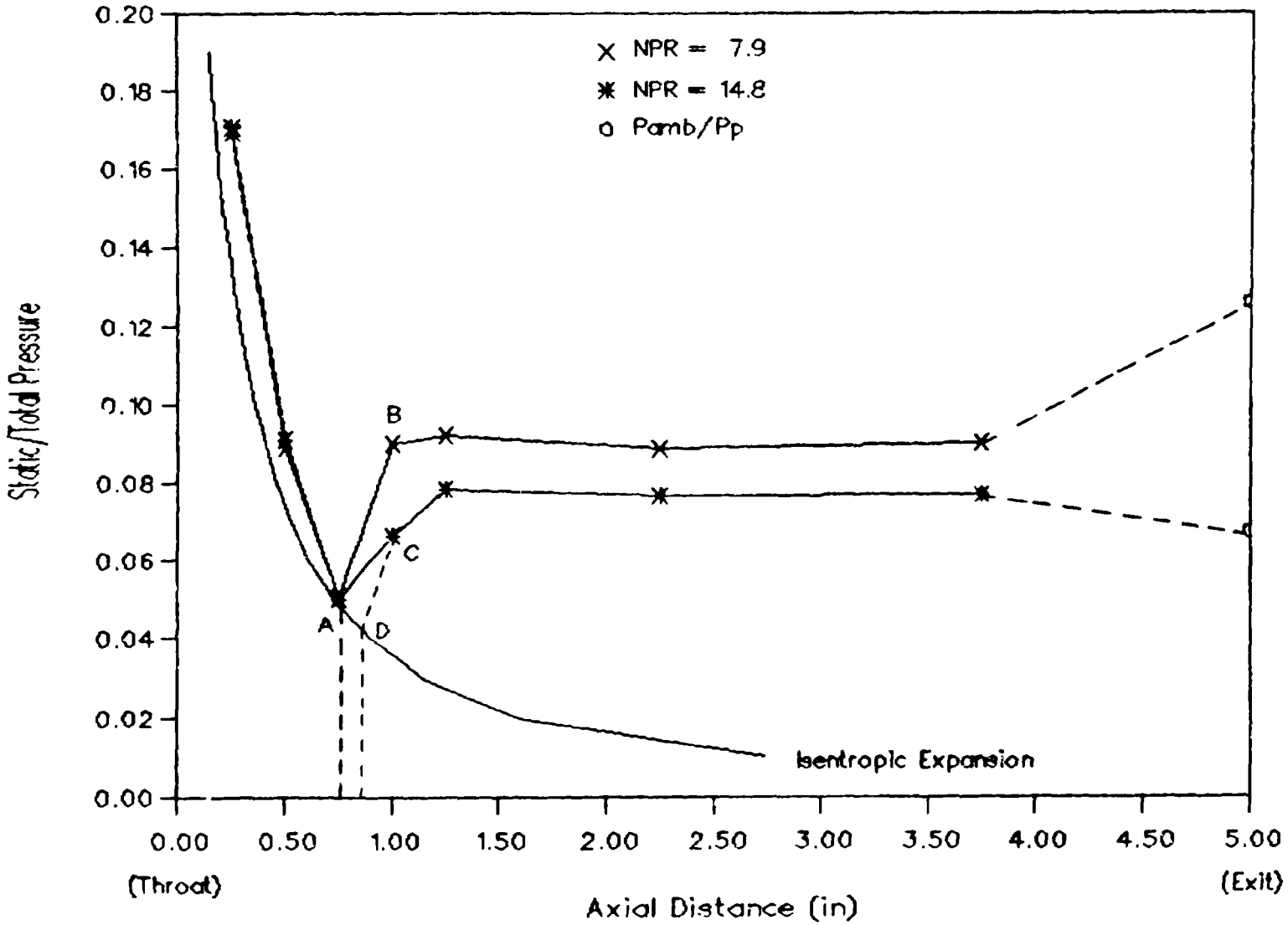

Figure 38 Static Pressure Distribution, Nozzle 53528, No Secondary Ports

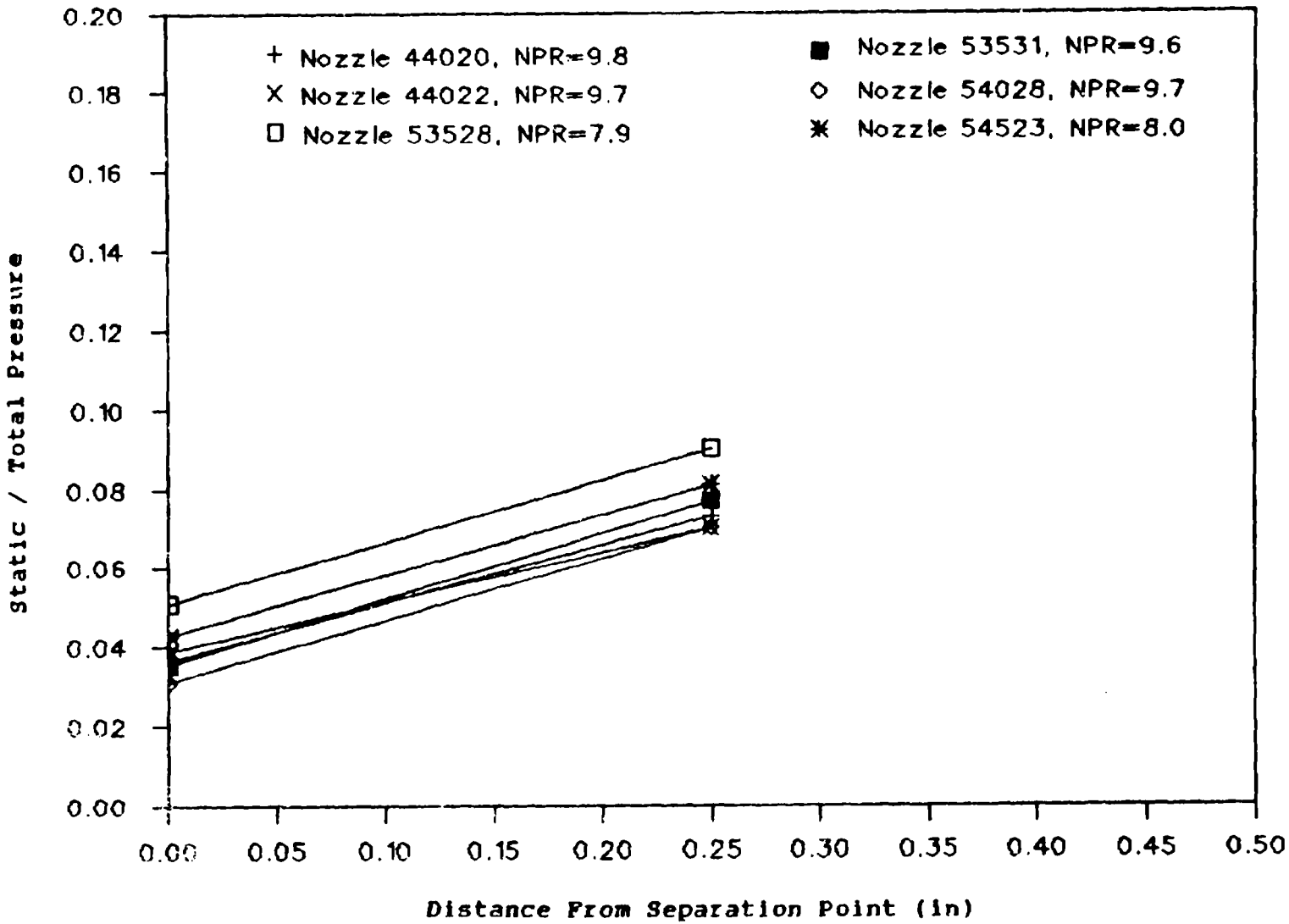

Figure 39 Pressure Gradient Downstream of Separation Point

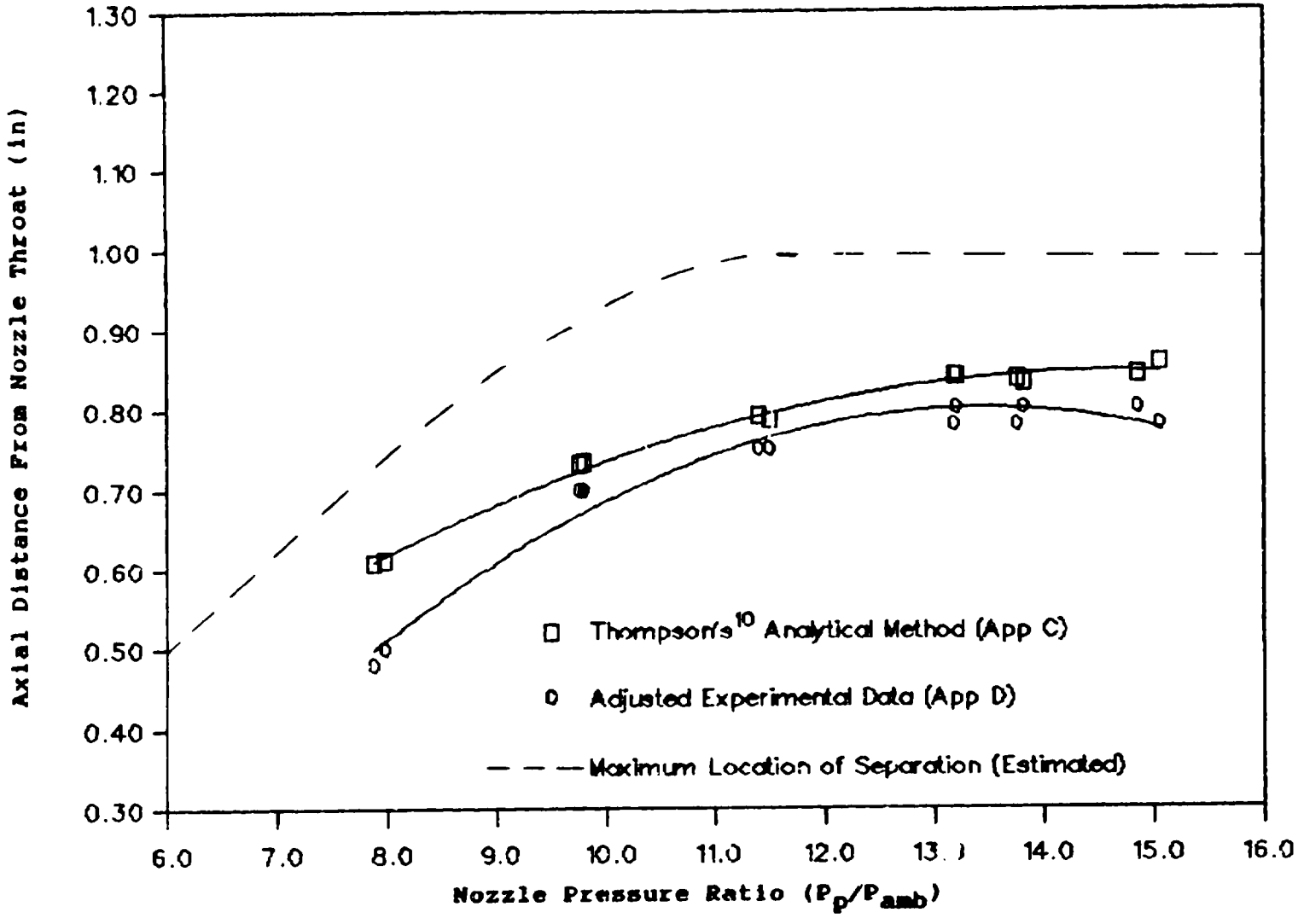

Figure 40. Flow Separation Point, Comparison of Measured and Analytical Results, Nozzle 44020, No Secondary Ports

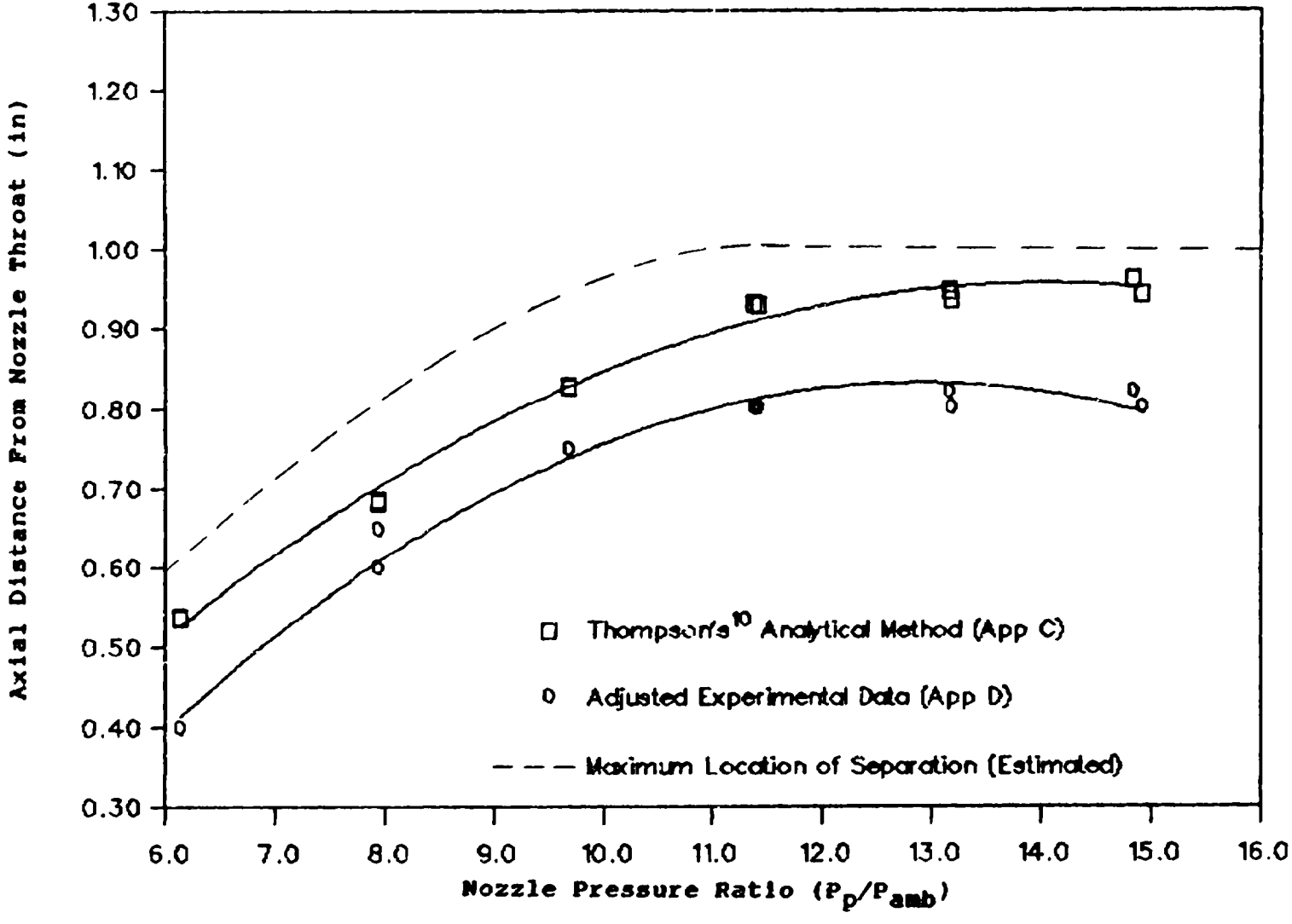

Figure 41. Flow Separation Point, Comparison of Measured and Analytical Results, Nozzle 44022, No Secondary Ports

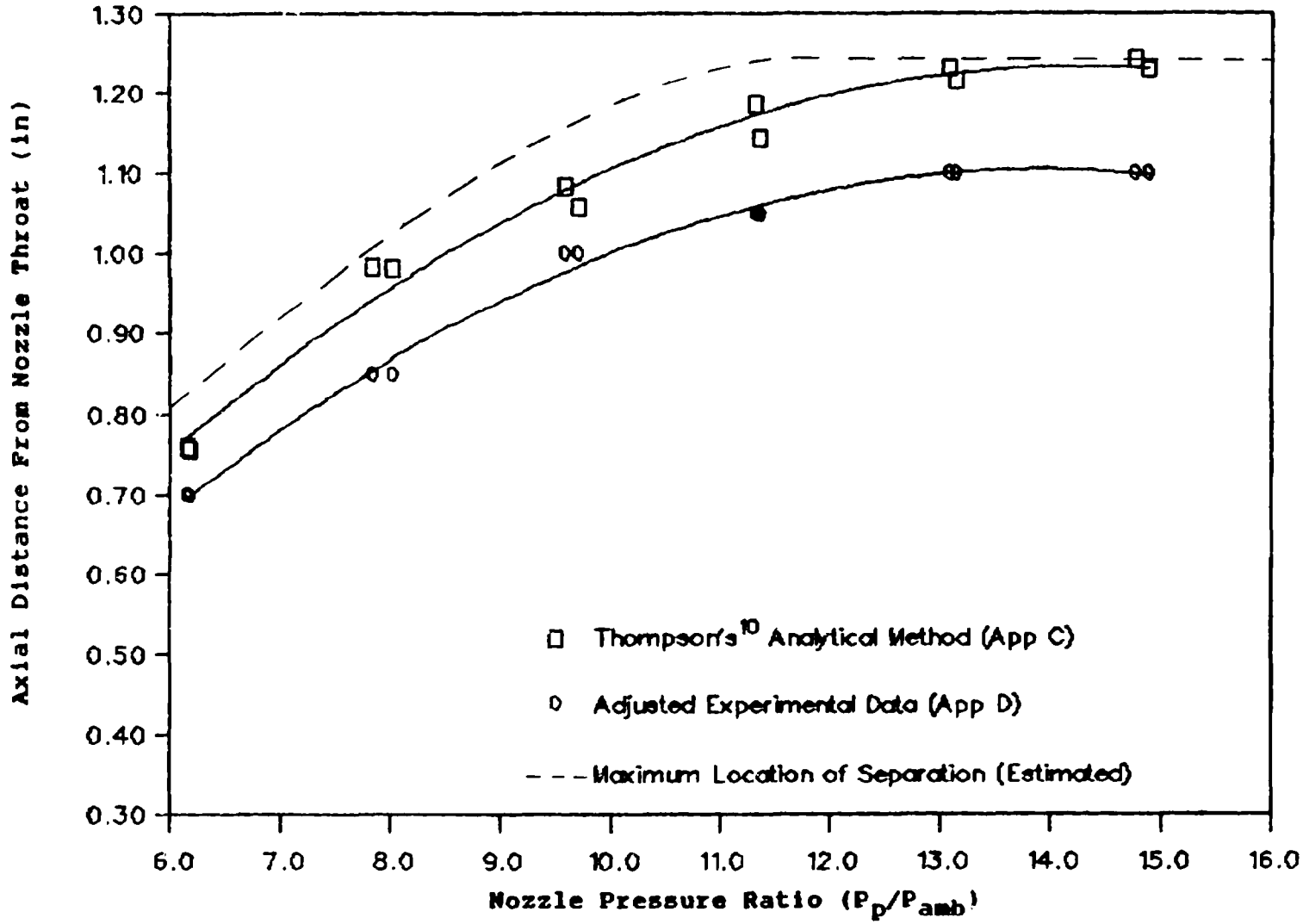

Figure 42. Flow Separation Point, Comparison of Measured and Analytical Results, Nozzle 53531, No Secondary Ports

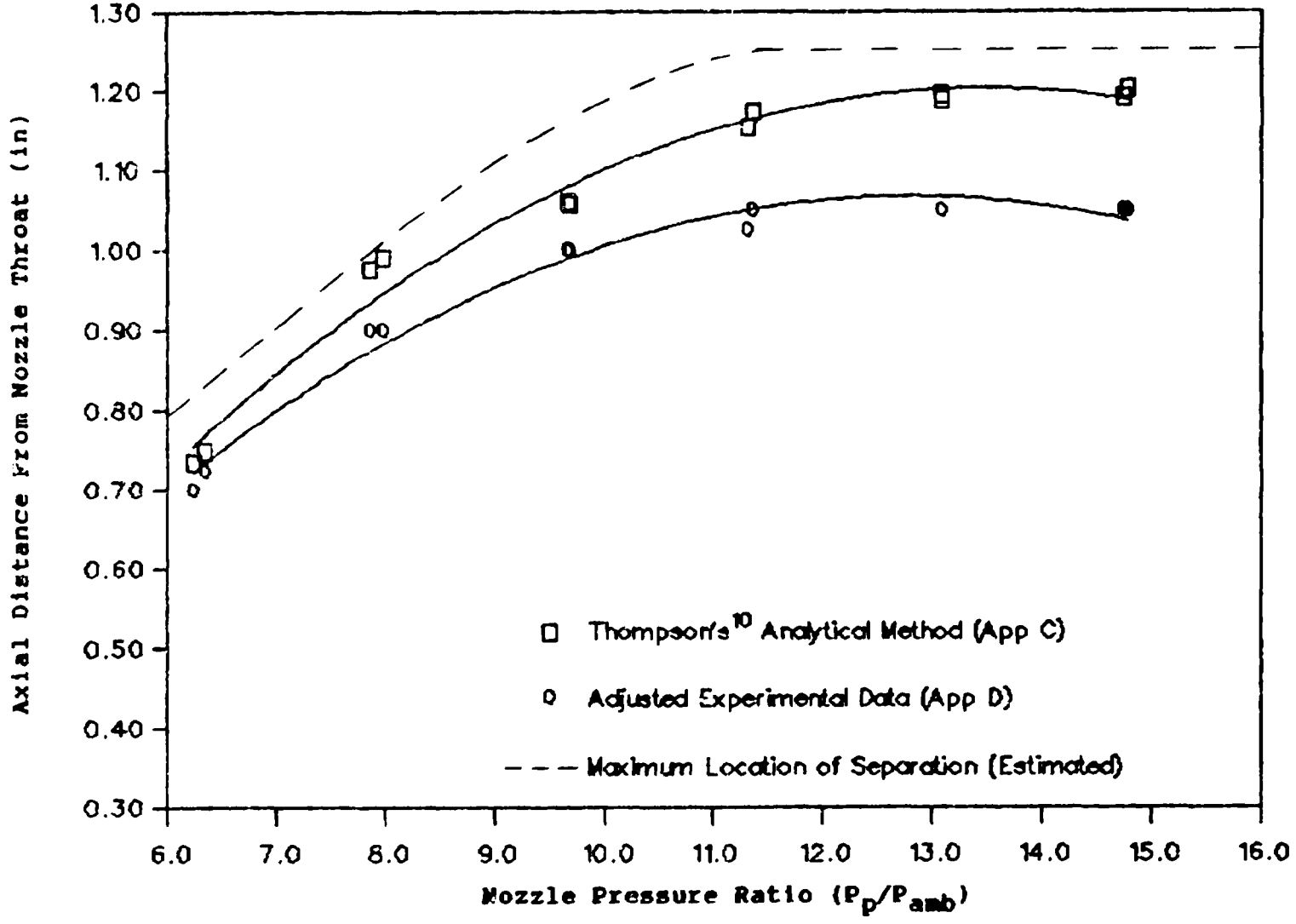

Figure 43. Flow Separation Point, Comparison of Measured and Analytical Results, Nozzle 54028, No Secondary Ports

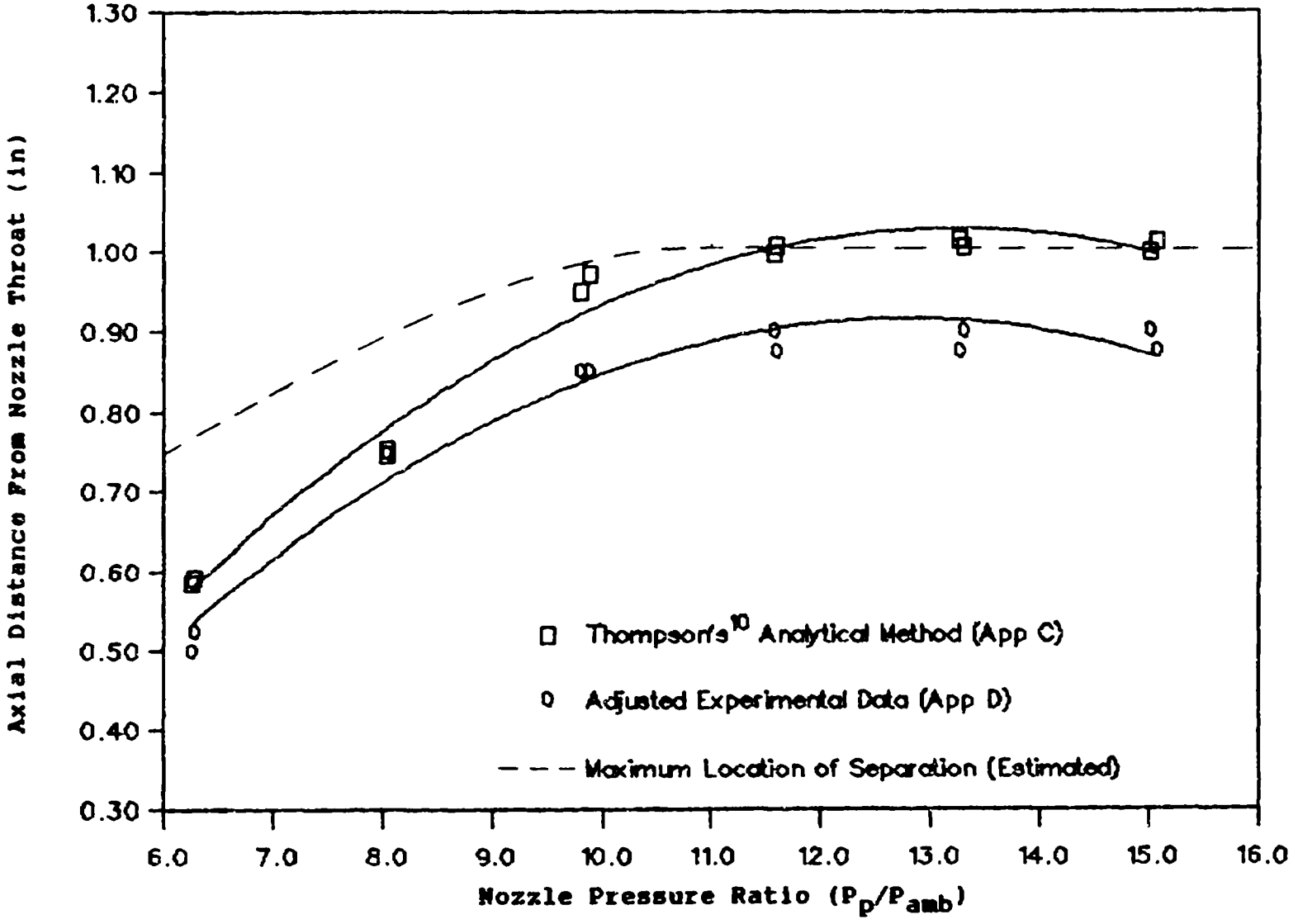

Figure 44. Flow Separation Point, Comparison of Measured and Analytical Results, Nozzle 54523, No Secondary Ports

Bibliography

1. Carroll, G.R. and H. Cox, "A Missile Flight Control System Using Boundary Layer Thrust Vector Control," AIAA/SAE/ASME 19th Joint Propulsion Conference AIAA-83-1149. American Institute of Aeronautics and Astronautics, New York, 1983.

2. Cates, Captain James W., Two-Dimensional Confined Jet Thrust Vector Control with Flow Visualization and Variable Flow Geometry. MS Thesis AFIT/GA/AA/85D-2. School of Engineering, Air Force Institute of Technology (AU), Wright-Patterson AFB OH, December 1985.

3. Fitzgerald, R. E. and R. F. Kampe, "Boundary Layer TVC for Missile Applications," AIAA/SAE/ASME 19th Joint Propulsion Conference, AIAA-83-1153, American Institute of Aeronautics and Astronautics, New York, 1983

4. Friddell, J. H. and M.E. Franke, "Confined Jet Thrust Vector Control Nozzle Studies," AIAA/SAE/ASME/ASEE 26th Joint Propulsion Conference, AIAA-90-2027, American Institute of Aeronautics and Astronautics, Washington, D. C., 1990.

5. Lambert, P.G. and M.E. Franke, "Characteristics of Axisymmetric Confined Jet Thrust Vector Control," AIAA/ASME/SAE/ASEE 24th Joint Propulsion Conference, AIAA-88-3237, American Institute of Aeronautics and Astronautics, Washington, D.C., 1988.

6. Porzio, A.J. and M.E. Franke, "Experimental Study of a Confined Jet Thrust Vector Control Nozzle," Journal of Propulsion and Power, Vol. 5, No. 5, Sept.-Oct. 1989, pp. 596-601.

7. Scheller, K. and J.A. Bierlein, "Some Experiments on Flow Separation in Rocket Nozzles," ARS Journal, Jan.- Feb. 1953, pp. 28-32.

8. Sutton, G. P. Rocket Propulsion Elements. New York: John Wiley and sons, 1986.

9. Talda, Second Lieutenant Timothy A., Experimental Investigation of Two-Dimensional Confined Jet Thrust Vector Control. MS Thesis AFIT/GAE/AA/87D-22. School of Engineering, Air Force Institute of Technology (AU), Wright-Patterson AFB OH, December 1987.

10. Thompson, R.V., "Theoretical Determination of the Point of Separation in a Compressible, Turbulent, Supersonic Boundary Layer Subjected to an Adverse Pressure Gradient," Paper No. 67-WA/FE-38, The American Society of Mechanical Engineers, New York NY, 1967.

VITA

Timothy Hawkes graduated from high school in Madelia, MN in 1979. He attended the University of Minnesota and received the degree of Bachelor of Aerospace Engineering and Mechanics in June 1984. After graduation he was employed by The Boeing Company as an engineer working on the propulsion systems for the Boeing 747 and 767 airplanes. In 1988 he left The Boeing Company to work in the Aero-Propulsion and Power Laboratory, Turbine Engine Division at Wright-Patterson AFB, where he serves as program manager for Exploratory Development (6.2) and Advanced Development (6.3) programs in the area of propulsion integration. Shortly after stating work he enrolled in the School of Engineering, Air Force Institute of Technology as a part time student.

Permanent address: 4166 Whitegate Dr
Beavercreek, OH 45430

REPORT DOCUMENTATION PAGE

Form Approved
OMB No. 0704-0188

1. AGENCY USE ONLY (Leave blank)	2. REPORT DATE	3. REPORT TYPE AND DATES COVERED
	June, 1991	MS Thesis

4. TITLE AND SUBTITLE
Experimental Evaluation of Design Variables for Two-Dimensional Confined Jet Thrust Vector Control Nozzles

5. FUNDING NUMBERS

6. AUTHOR(S)
Timothy M. Hawkes

7. PERFORMING ORGANIZATION NAME(S) AND ADDRESS(ES)
School of Engineering (AFIT/ENY)
Air Force Institute of Technology
Wright-Patterson AFB OH 45433-6583

8. PERFORMING ORGANIZATION REPORT NUMBER
AFIT/GAE/ENY/91J-1

9. SPONSORING MONITORING AGENCY NAME(S) AND ADDRESS(ES)

10. SPONSORING MONITORING AGENCY REPORT NUMBER

11. SUPPLEMENTARY NOTES

12a. DISTRIBUTION AVAILABILITY STATEMENT
Approved for Public Release;
Distribution Unlimited

12b. DISTRIBUTION CODE

13. ABSTRACT (Maximum 200 words)

Thesis Advisor: Dr. Milton E. Franke, AFIT/ENY

An experimental study of the axial and vectoring performance of two-dimensional (2-D) confined jet thrust vector control (CJTVC) nozzles was performed. The effects of adding secondary injection ports and changing exit height and secondary injection port location were studied on several 2-D CJTVC nozzles. The axial and vectoring performance results for these nozzles were measured over a range of pressure ratios. An analytical method for predicting flow separation was found to be applicable to these nozzles. Guidelines for designing 2-D CJTVC nozzles, that can be vectored using secondary injection, were established. Recommendations for further study are made.

14. SUBJECT TERMS	15. NUMBER OF PAGES
Thrust Vectoring Nozzles; Secondary Injection; Two-Dimensional; Thrust Vector Control System	99
	16. PRICE CODE

17. SECURITY CLASSIFICATION OF REPORT	18. SECURITY CLASSIFICATION OF THIS PAGE	19. SECURITY CLASSIFICATION OF ABSTRACT	20. LIMITATION OF ABSTRACT
Unclassified	Unclassified	Unclassified	